ΔSH3 (lacking aa 1–60), NEDD9 ΔSD (lacking aa 63–401), NEDD9 ΔC (lacking aa 406–834), NEDD9 ΔYDYVHL (lacking aa 629–834), NEDD9 ΔCC (lacking aa 637–834), NEDD9 ΔHLH (lacking aa 707–834), and NEDD9 F in which Y629 and Y631 were mutated into F. The plasmids were transfected into cells using Lipofectamine 2000 (Invitrogen) or FuGENE6 (Roche Applied Science) according to the manufacturer's instructions. In experiments using BCMG hygro vectors, transfected cells were selected in 0.2 mg/mL hygromycin B to establish stable transformants. The expression vector pMX-luc/neo for firefly luciferase was described elsewhere (34).

Gene knockdown by siRNA

To deplete endogenous NEDD9 or BCAR1, Stealth RNAi siRNAs were obtained from Life Technologies. The target sequence of siRNA for NEDD9 is 5′-UCCCAUGCAGGAGACUGCCUCCAGU-3′ and that for BCAR1 is 5′-GCCUCAAGAUCUUGGUGGGCAUGUA-3′. As a control, we used Stealth RNAi siRNA negative control. The siRNAs were transfected using Lipofectamine RNAiMAX transfection reagent according to the manufacturer's instructions (Life Technologies).

Protein extraction, immunoprecipitation, and immunoblotting

Cells were serum-starved for 24 hours before the treatment with EGF (at a final concentration of 10 ng/mL). For suspension culture, HydroCell low cell binding culture dish (CellSeed Inc.) was used with serum-free medium. Cytoplasmic protein extracts were prepared by detergent lysis (1% Triton X-100) containing phosphatase and protease inhibitors. For immunoprecipitation, cell lysates were incubated with the appropriate first antibody at 4°C overnight and then with protein A Sepharose beads for 4 hours. After wash with lysis buffer, the beads were boiled in the SDS-PAGE loading buffer. The immunoprecipitates and cell lysates were separated by 8% SDS-PAGE gels and electrophoretically transferred onto polyvinylidene difluoride membranes. After blocking, the membranes were incubated serially with the primary antibody and horseradish peroxidase (HRP)-conjugated secondary antibody and then developed by enhanced chemiluminescence system (GE Healthcare).

Cell migration and invasion assays

Cell migration assay was conducted as described previously using Transwell inserts (8-μm pore size; Corning Incorporated; ref. 24). Cells were placed in the upper chamber at 1×10^5 cells/mL in 100 μL of 0.6% bovine serum albumin (BSA)/RPMI-1640 medium. After 6 hours, the inserts were fixed and stained with Diff-Quick. The cells that had not migrated were removed from the upper surface of the inserts using cotton swabs. Images of 3 different high-power fields were captured from each insert, and the number of migratory cells was counted. To determine invasive potential, Matrigel invasion chamber (BD BioCoat) was used.

Animals

Five- to 6-week-old female NOD/Shi-scid, IL-2Rγ^{null} mice (NOG mice; ref. 35) were supplied from Central Institute for Experimental Animals (Kawasaki, Japan) and maintained in a specific pathogen-free facility. All experiments were approved by and carried out following the guidelines of the Institute Animal Care and Use Committee of the University of Tokyo (Tokyo, Japan).

In vivo bioluminescence imaging

Human NSCLC cell line PC-14 was transplanted subcutaneously into the lumbar region on the dorsal side of NOG mice. On days 21 and 28, progression of the transplanted tumors was monitored by the following bioluminescence imaging (BLI) technique. D-Luciferin (Beetle Luciferin Potassium Salt; Promega) was used as the substrate for the luciferase expressed by PC-14 cells. The mice received an intraperitoneal injection of 150 mg/kg D-luciferin and placed in the light tight chamber of a cooled CCD camera system (IVIS Imaging System 100; Xenogen) in the prone position under isoflurane anesthesia. Dorsal, left lateral, ventral, and right lateral images were acquired from 10 minutes after D-luciferin injection with the CCD camera system. All luminescent images were collected with an exposure time of 1 minute and binning of 8.

Gross and microscopic pathology

The NOG mice undergoing xenograft transplantation were euthanized with carbon dioxide on day 28 after BLI. Major organs were examined for grossly visible changes. Lung tissues and the primary tumors were removed into 10% neutral-buffered formalin for histology. After formalin fixation, samples were processed into paraffin wax, sectioned at a nominal thickness of 5 μm, stained with hematoxylin and eosin (H&E), and examined by light microscopy.

Clinical specimens and immunohistochemical staining

Upon approval from the Institutional Review Board of Keio University (Tokyo, Japan), we selected 60 consecutive patients with lung adenocarcinoma treated with curative surgery resection between 1999 and 2001 from the Keio University Hospital (IRB number: 16–90). Immunohistochemical studies were conducted on 5-μm sections of formalin-fixed, paraffin-embedded tissue section of the primary tumors of lung. Antigen retrieval was conducted with 0.01 mol/L of boiled citrate buffer (pH 9.0) for 10 minutes. The slides were stained on the Dako Autostainer (Dako) using the EnVision (Dako) staining reagents. The sections were first blocked for endogenous protein binding and peroxidase activity with Dual Endogenous Block (Dako) for 10 minutes. The sections were serially incubated with a polyclonal antibody against NEDD9 (2 μg/mL) and EnVision+ Dual Link reagent for 30 minutes. The sections were then treated with 3,3′-diaminobenzidine (DAB) and hydrogen peroxide. A toning solution (DAB Enhancer, Dako) was used to enrich the final color. The sections were counterstained with hematoxylin, dehydrated, and

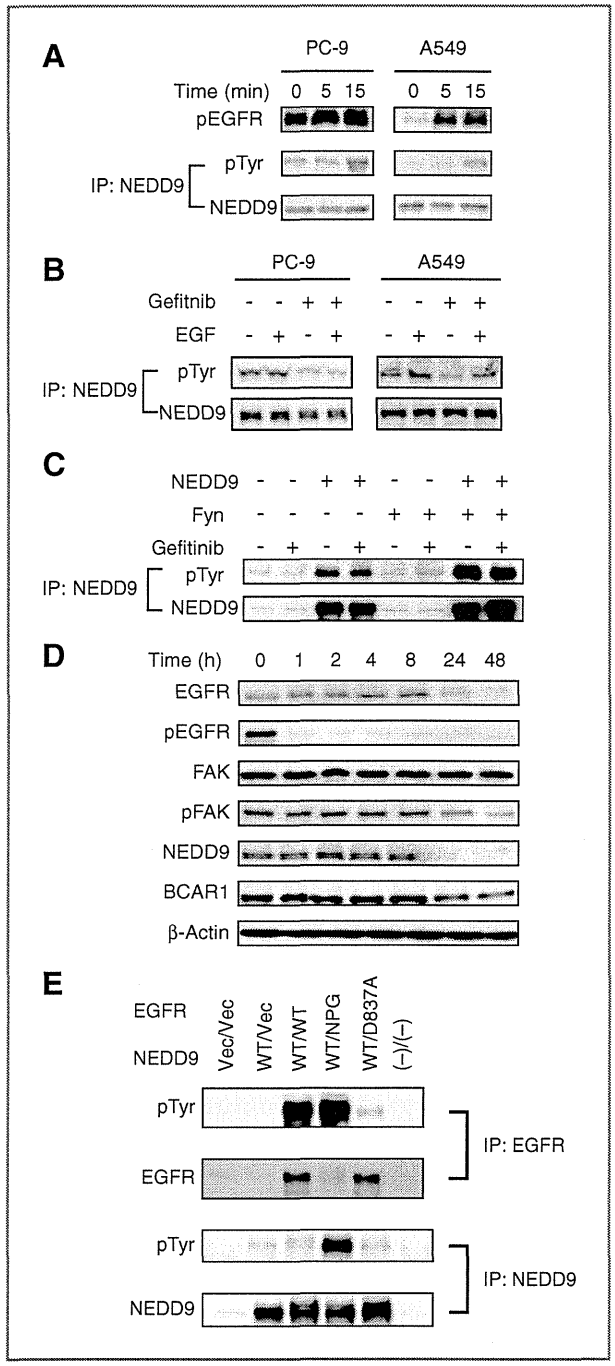

Figure 1. A, EGF stimulation promotes phosphorylation of NEDD9 in human NSCLC cell lines. PC-9 cells and A549 cells were treated with EGF (10 ng/mL) for the indicated time period and then the cells were lysed by scraper in the lysis buffer. Lysates were immunoprecipitated with anti-NEDD9 pAb. The lysates and immunoprecipitates were subjected to immunoblotting with the indicated antibodies. IP, immunoprecipitate; NEDD9, anti-NEDD9 mAb; pEGFR, anti-phospho-EGFR pAb; pTyr, anti-phosphotyrosine mAb. B, inhibition of EGFR by gefitinib downregulates tyrosine phosphorylation of NEDD9 in NSCLC cell lines. PC-9 and A549 cells were cultured in the presence or absence of gefitinib (0.2 μmol/L) for 2 hours and the cells were then treated in the same manner as A. C, gefitinib does not inhibit Fyn-mediated tyrosine phosphorylation of NEDD9 in 293T cells. 293T cells (6×10^6 cells) were transfected with expression plasmid pSRα NEDD9 (NEDD9) and/or pME18S Fyn (Fyn) by FuGENE6. After 48 hours, the cells were lysed and immunoprecipitated with anti-NEDD9 pAb. Treatment with gefitinib (0.2 μmol/L) was conducted during 2 hours before the cell lysis. The immunoprecipitates were subjected to immunoblotting with the indicated antibodies. D, inhibition of EGFR by gefitinib modulates FAK, NEDD9, and BCAR1 in PC-9 cells. PC-9 cells were treated with 0.2 μmol/L gefitinib for the indicated time period. The cells were lysed by scraper in the lysis buffer. The lysates were then subjected to immunoblotting with the indicated antibodies. BCAR1, anti-BCAR1 mAb; β-actin, anti-β-actin mAb; EGFR, anti-EGFR pAb; FAK, anti-FAK mAb; NEDD9, anti-NEDD9 mAb; pFAK, anti-phospho-FAK Ab. E, constitutively active EGFR tyrosine phosphorylates NEDD9 in 293T cells. 293T cells (6×10^6 cells) were co-transfected with pBabe puro EGFR (wild-type or mutants) and pSRα NEDD9 (wild-type) by FuGENE6. At 24 hours after transfection, the cells were detached by trypsin/EDTA and cultured in suspension with serum-starved condition. At 48 hours after transfection, the cells were lysed and immunoprecipitated with anti-NEDD9 pAb or anti-EGFR pAb. The immunoprecipitates were subjected to SDS-PAGE and immunoblotting with the indicated antibodies. Combination of the vectors is as follows: Vec/Vec, pSRα/pBabe puro; WT/Vec, pSRα NEDD9/pBabe puro; WT/WT, pSRα NEDD9/pBabe puro EGFR WT; WT/NPG, pSRα NEDD9/pBabe puro EGFR NPG (constitutively active); WT/D837A, pSRα NEDD9/pBabe puro EGFR D837A (kinase dead); (–)/(–), no plasmids (FuGENE6 alone).

coverslipped. Immunostaining for each sample was determined to be positive (defined as ≥30% positive cells) or negative (<30% positive cells) in a blind fashion by the participating pathologist. We compared 3 cutoff values for NEDD9 positivity (10%, 30%, and 50%) and chose 30%.

Statistical analysis

The χ^2 analysis was applied for the comparison of dichotomous variables. The Kaplan–Meier estimate was used for recurrence-free survival (RFS) and overall survival (OS) analysis, and the log-rank test was used to compare the difference. The Cox proportional hazards model was applied in univariate and multivariate survival analysis to test independent prognostic factors. The control groups of all statistical analyses were usually the first groups in the panels unless specified otherwise in the figure legends. All the statistical analyses were conducted by SPSS Statistics 17 (IBM Corporation) at the 0.05 level of significance.

Clinical investigation was conducted according to Declaration of Helsinki principles. The written informed consent was received from patients before inclusion in this study.

Results

EGF enhances NEDD9 tyrosine phosphorylation

To examine the role of NEDD9 in EGFR signaling pathway in NSCLCs, we first used NSCLC cell lines PC-9 and A549. As shown in Fig. 1A, stimulation with EGF elevated the level of tyrosine phosphorylation of NEDD9 in both PC-9 and A549 cells. Because PC-9 harbors activating mutation of EGFR (ΔE746-A750), the basal level of tyrosine phosphorylation of endogenous EGFR was significantly higher than that of A549 cells with the wild-type EGFR. A TKI for EGFR, gefitinib, abolished the increase in tyrosine phosphorylation of NEDD9 induced by EGF in those cells (Fig.

1B). To assess the specificity of EGFR-mediated tyrosine phosphorylation of NEDD9, we next used the human embryonic kidney cell line 293T cells. As shown in Fig. 1C, gefitinib did not alter the level of tyrosine phosphorylation of NEDD9 caused by exogenous Fyn, an Src family tyrosine kinase in 293T cells. Time course experiments showed that the treatment of PC-9 cells with gefitinib downregulated not only tyrosine phosphorylation of EGFR but also that of FAK. Interestingly, the protein amounts of EGFR, NEDD9, and NEDD9 homologue BCAR1 were also reduced following the addition of gefitinib (Fig. 1D).

In NSCLCs, a variety of activating mutations or deletions have been found in EGFR to correlate with poor clinical outcome. To evaluate the effect of such gene alterations on the tyrosine phosphorylation of NEDD9 *in vitro*, we next conducted co-transfection analysis using 293T cells in suspension culture with serum starvation. As a result, co-transfection of constitutively active mutant EGFR D770-N771 (EGFR NPG) promoted significant level of tyrosine phosphorylation of NEDD9 despite its relatively low level of protein expression, whereas other EGFR constructs including wild-type EGFR and the kinase-negative mutant D837A did not alter the level of tyrosine phosphorylation of NEDD9 (Fig. 1E). However, immunoprecipitation and co-localization analysis revealed that these EGFR constructs and NEDD9 did not co-precipitate and co-localize only marginally (data not shown). These results therefore suggest that the EGFR signaling pathway may modulate tyrosine phosphorylation of NEDD9 in an indirect manner.

Exogenous NEDD9 enhances migratory and invasive potential of NSCLC cell lines

We previously showed that transfected NEDD9 upregulated the motility of Jurkat T cell line on fibronectin (FN) and/or anti-CD3 mAb (23). To determine the association between the expression level of NEDD9 and migratory or invasive behavior of NSCLCs, we used full-length construct for NEDD9, a point mutant NEDD9 F in which the Src SH2-binding motif YDYVHL was mutated to FDFVHL, and a series of deletion mutants: NEDD9 ΔSH3 lacking N-terminal SH3 domain (binding site for FAK and Pyk2); NEDD9 ΔSD lacking the substrate domain (binding site for Crk, Nck), NEDD9 ΔC lacking the C-terminal half, NEDD9 ΔYDYHL lacking from the C-terminus to the YDYVHL motif, NEDD9 ΔCC lacking from the C-terminus to the coiled-coil domain, NEDD9 ΔHLH lacking from the C-terminus to the helix-loop-helix domain (24). The structures of these mutants were schematically summarized in Fig. 2A. In Fig. 2B, we showed the protein expression of these constructs of NEDD9 in the A549 stable transformants.

As shown in Fig. 2C–F, gene transfer of the wild-type NEDD9 into PC-9 and A549 conferred significant enhancement of cell motility (Fig. 2C and D), as well as increasing their invasive potential into Matrigel, which is rich in basement membrane proteins (Fig. 2E and F). This enhancement of EGF- or EGF/integrin-mediated cell migration and invasion was markedly reduced by the addition of gefitinib, suggesting the importance of EGF/EGFR signaling in metastasis and invasion of NSCLCs. Of particular interest is that addition of gefitinib also reduced the fibronectin-mediated cell migration in the absence of exogenous EGF (Figs. 2C and D and 3C and D), suggesting a possible role for NEDD9 in the crosstalk of integrin and EGFR.

We next conducted migration assay of A549 cells with a set of NEDD9 mutants in the presence of EGF (Fig. 2G). As shown in the figure, deletion of SH3, SD domain, or the domains from C-terminus to SD abolished the motility-enhancing effect of NEDD9 completely. On the other hand, mutation or deletion of Src SH2-binding motif reduced this activity in a less efficient manner. The set of experiments involving serial C-terminal deletions suggest that the C-terminal region (CT) may regulate the biologic effect of NEDD9 to a certain degree. These results also show that exogenous expression of NEDD9 promotes cancer cell migration and invasion. In addition, the SH3, SD, and SR domains of NEDD9 are particularly important for EGF/integrin-induced cell motility.

Gene ablation of NEDD9 or BCAR1 reduces the migratory and invasive activity of NSCLC cell lines

To further confirm the enhancing effect of NEDD9 on cell motility and invasiveness of NSCLCs, we conducted gene knockdown studies involving endogenous NEDD9 and its related protein BCAR1 by transfecting PC-9 and A549 with their respective siRNA. Concerning to the off-targeting effect, we evaluated 3 siRNAs (siRNA-1: UCCCAUGCAGGAGACUGCCUCCAGU, siRNA-2: UCCCAGGCAACCGGGUGAAGCUUCU, and siRNA-3: CCUUAUAUGACAAUGUCCCAGAGUG) for NEDD9 in their inhibitory effects and in cDNA rescue experiments and selected siRNA-1 (Supplementary Fig. S1).

As shown in Fig. 3, introduction of NEDD9-specific siRNA abolished not only fibronectin-induced cell migration and invasion but also EGF-induced cell invasion. The BCAR1-specific siRNA also reduced cell migration and invasion, although its inhibitory effect was less than that of NEDD9-specific siRNA in NSCLC cell lines.

Together, results of the gene transfer and gene knockdown experiments suggest that NEDD9 as well as BCAR1 seem to be indispensable factors for EGF as well as integrin-mediated cell motility and invasiveness in NSCLCs.

Gene transfer of NEDD9 into an NSCLC cell line promotes lung metastasis *in vivo*

Our data showing the enhancing effects of NEDD9 on cell motility and invasion of NSCLC cell lines led us to evaluate a xenograft transplantation model using immunodeficient mice (NOG mice) and BLI (34). For this purpose, we used the poorly differentiated human lung adenocarcinoma cell line PC-14 which is negative for NEDD9 at the protein level (Fig. 4A). Figure 4B shows stable expression of transfected NEDD9 (wild-type) in PC-14 cells as long as 28 days after xenotransplantation into NOG mice. The bioluminescence images of xenograft-transplanted NOG mice revealed a positive signal in the lung region of mice transplanted with

Published OnlineFirst October 4, 2012; DOI:10.1158/1078-0432.CCR-11-2162

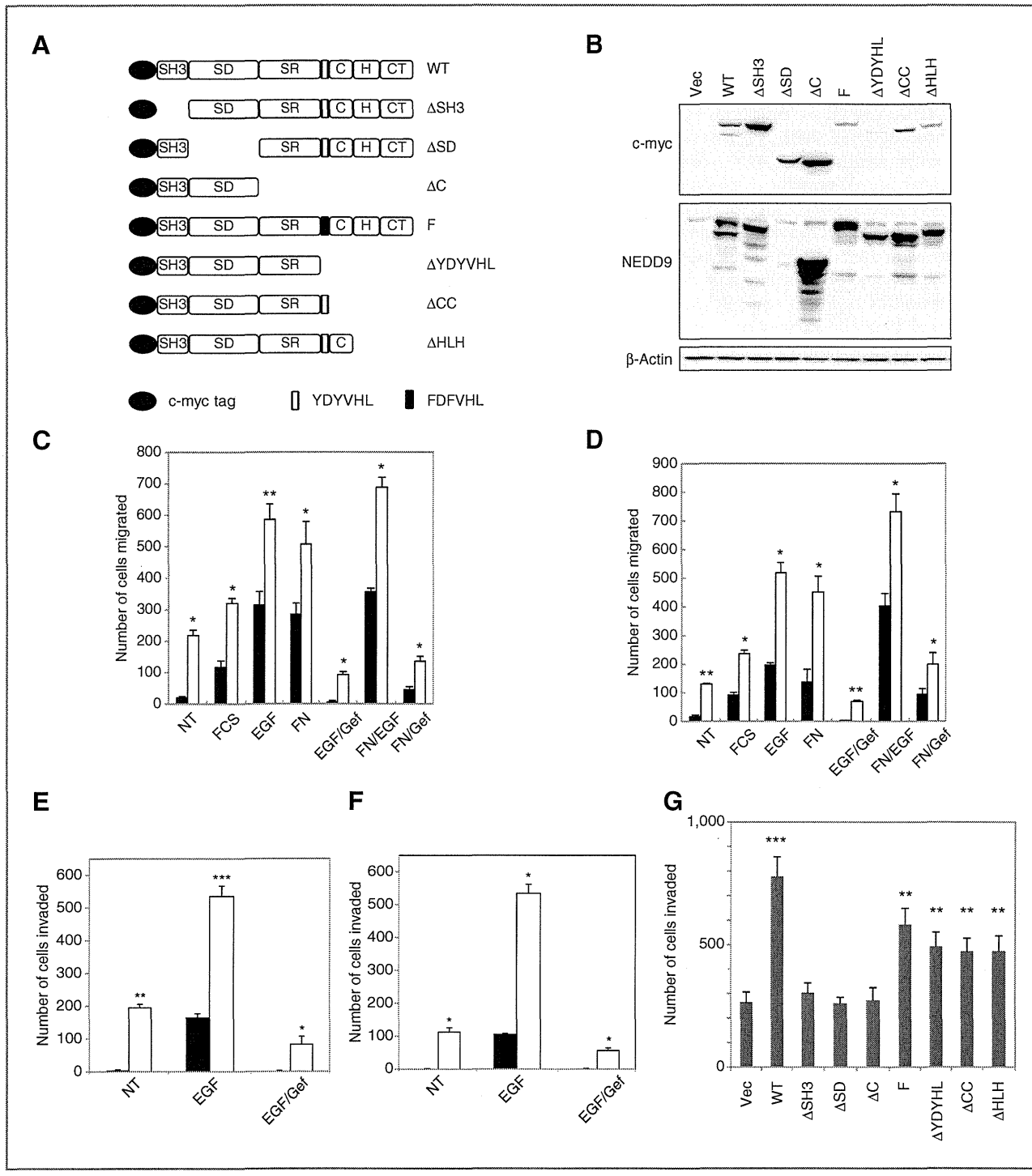

Figure 2. Exogenous NEDD9 enhances migratory and invasive potential of NSCLC cell lines. A, structure of NEDD9 and its mutants. The secondary structure of NEDD9 is graphically shown. From 5′, closed oval, c-myc tag; SH3, Src homology 3 domain; SD, substrate domain; SR, serine-rich region; C, coiled-coil domain; H, helix-loop-helix domain; CT, C-terminal region. B, protein expression of NEDD9 and its mutants in A549 NEDD9 transfectants. A549 cells were transfected with the indicated NEDD9 constructs. After establishing stable transformants, the cell lysates were subjected to immunoblotting with the indicated antibodies (c-myc, anti-c-myc mAb). Vec, BCMG hygro. C–F, transfection of wild-type NEDD9 promotes migratory activity of NSCLC cell lines. PC-9 (C and E) and A549 cells (D and F) were transfected with either empty vector BCMG hyg (closed bar) or BCMG hyg c-myc NEDD9 WT (open bar). The stable transformants were subjected to cell migration assay (C and D) or cell invasion assay (E and F) in the presence or absence of the indicated reagents. NT (nontreated), fetal calf serum (FCS), 10% in the lower chamber; EGF, 10 ng/mL in the lower chamber; FN, inserts were coated with 0.5 μg/mL of fibronectin; Gef, gefitinib in both chambers at 0.2 μmol/L. Statistical significance was evaluated by comparison with NT. *, $P < 0.01$; **, $P < 0.001$; ***, $P < 0.0001$. G, motility-enhancing effect of a series of NEDD9 mutants. A549 NEDD9 transfectants were subjected to the cell migration assay in the presence of EGF (10 ng/mL). Statistical significance was evaluated by comparison with Vec (BCMG hygro).

Published OnlineFirst October 4, 2012; DOI:10.1158/1078-0432.CCR-11-2162

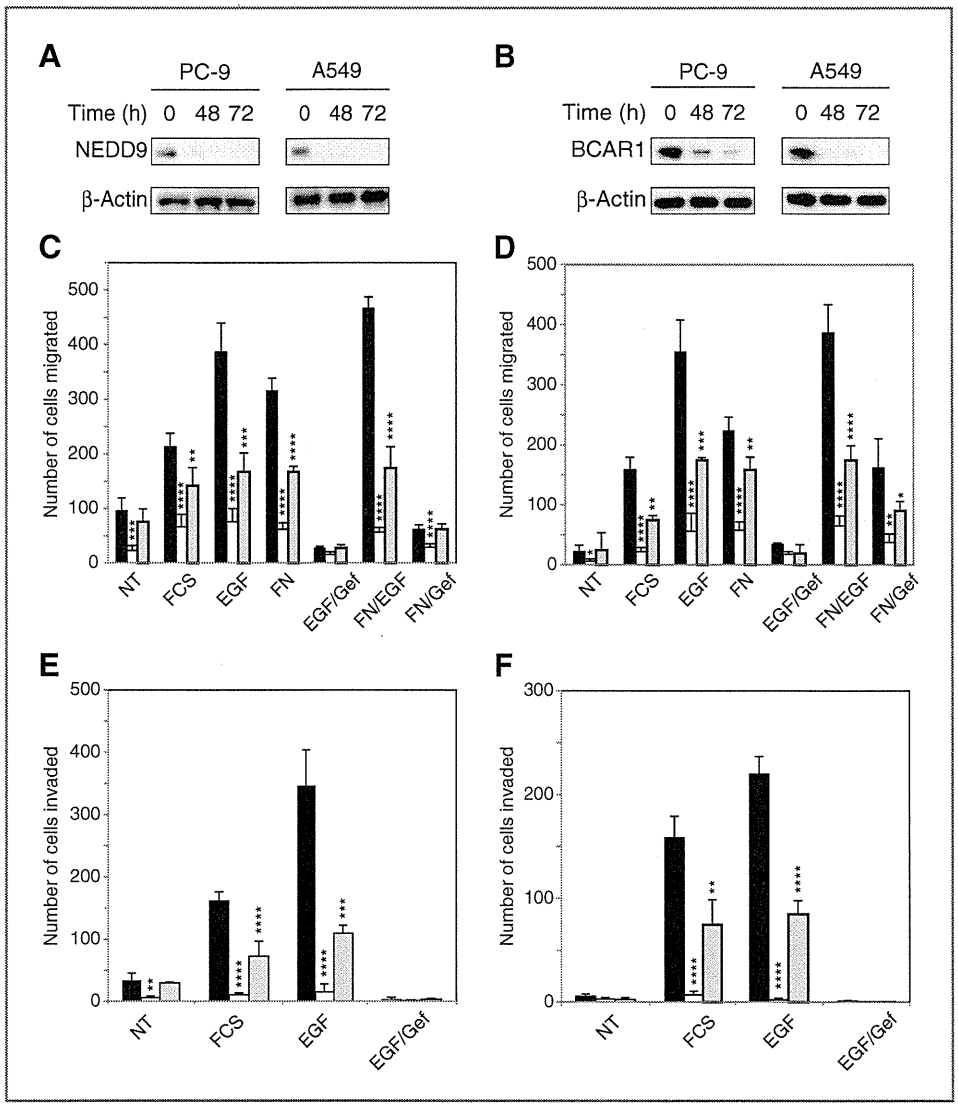

Figure 3. Gene ablation of NEDD9 reduces the migratory and invasive activity of NSCLC cell lines. A and B, protein expression levels of NEDD9 (A) and BCAR1 (B) in PC-9 and A549 cells transfected with their respective specific siRNAs. The cells were lysed 48 or 72 hours following transfection, and equivalent amounts of lysates were subjected to SDS-PAGE and blotted with the indicated antibodies. C–F, transfection of siRNA for NEDD9 or BCAR1 abolishes cell motility and invasiveness of NSCLC cell lines. PC-9 cells (C and E) and A549 cells (D and F) were transfected with siRNA for NEDD9 (open bar), BCAR1 (gray bar), or Stealth RNAi Negative Control (black bar) and subjected to cell migration assay (C and D) and cell invasion assay (E and F) in the presence or absence of the indicated reagents in the lower chamber. NT (nontreated control), fetal calf serum (FCS), 10%; EGF, 10 ng/mL in the lower chamber; FN (fibronectin), coated at 5 μg/mL; Gef (gefitinib), supplemented in both chamber at 0.2 μmol/L. Statistical significance was evaluated by comparison with negative control of each set of three data (Negative control, NEDD9 siRNA, and BCAR1 siRNA). *, $P < 0.05$; **, $P < 0.01$; ***, $P < 0.001$; ****, $P < 0.0001$.

PC-14 co-expressing luciferase and wild-type NEDD9 (Fig. 4C). A region of interest (ROI) of a fixed size was then set in the chest of these mice, and the mean signal intensity (photons/sec/cm^2/steradian) in the ROI was determined. In particular, for the mice transplanted with PC-14 co-expressing luciferase and wild-type NEDD9, the mean signal intensity of the ROI was $5.69 \times 10^3 \pm 0.64$ for the right lung and $10.33 \times 10^3 \pm 2.65$ for the left lung, whereas the mean signal intensity of the ROI was $1.23 \times 10^3 \pm 1.03$ for the right lung and $1.42 \times 10^3 \pm 0.66$ for the left lung of mice transplanted with control PC-14 cells expressing luciferase alone, a greater than 3 times higher signal intensity in the case with the PC-14 NEDD9 transformant. These results suggest that overexpression of NEDD9 promotes *in vivo* lung metastasis of a xenograft-transplanted NSCLC cell line in NOG mice. We next conducted metastasis assays in NOG mice with PC-14 NEDD9 mutants (ΔSH3 and ΔC). We found that subcutaneous injections of these cell lines resulted in detectable tumors in NOG mice. However, the sizes of the primary tumors were less than tumors created by PC-14 vector transfectant and NEDD9 wild-type transfectant. Furthermore, by microscopic examination, we could not detect any metastatic lesions in the lungs of these mice, indicating that these NEDD9 mutants displayed a dominant-negative effect on cell metastasis as well as tumor growth (Fig. 4D and E).

Expression of NEDD9 in human NSCLCs is associated with poor prognosis in lung cancer patients

To determine the clinical relevance of NEDD9 expression in human NSCLCs, we evaluated NEDD9 expression in the primary lesions of human lung adenocarcinoma and also examined the available clinical information of 60 patients treated consecutively at Keio University Hospital with curative surgery between 1999 and 2001. Clinical characteristics of these patients are summarized in Supplementary Tables S1 and S2. By immunohistochemical method, significant expression of NEDD9 protein was identified in 46.7% (28

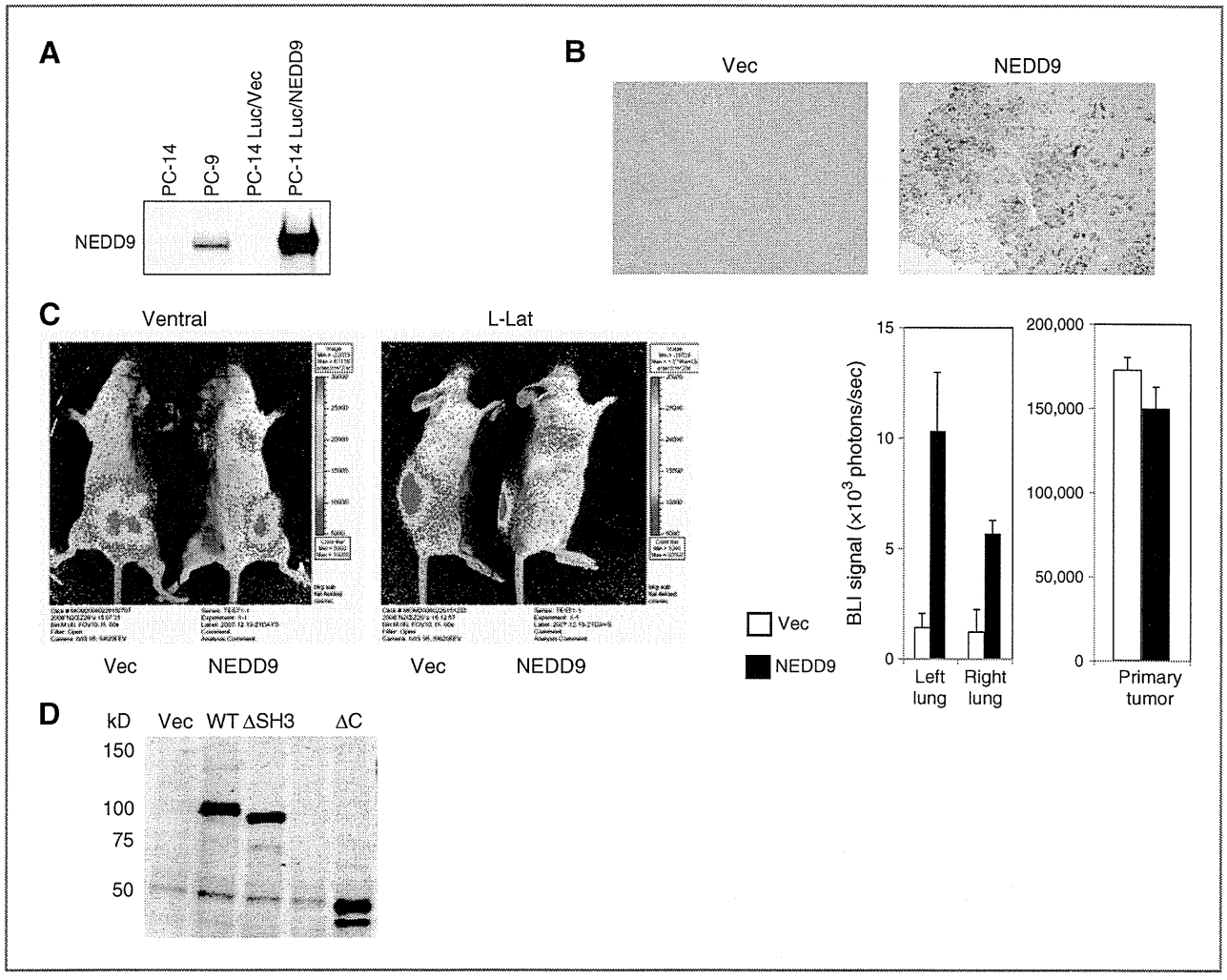

Figure 4. Gene transfer of NEDD9 into the NSCLS cell line PC-14 promotes lung metastasis in NOG mice. A, expression of transfected NEDD9 in PC-14 cells. PC-14 cells were serially transfected with pMX-luc/neo and BCMG hygro c-myc NEDD9 WT (PC-14 Luc/NEDD9) or pMX-luc/neo and BCMG hygro (PC-14 Luc/Vec) by Lipofectamine 2000. Stable clones were established by selection with G418 (1 mg/mL) and hygromycin B (0.2 mg/mL). The equivalent protein extracts from these transformants, parental PC-14 cells, and PC-9 cells were subjected to immunoblotting analysis with anti-NEDD9 mAb. B, immunohistochemical staining for NEDD9 in primary NSCLC tumors. NOG mice underwent subcutaneous transplantation of PC-14 Luc/Vec or PC-14 Luc/NEDD9. At necropsy on day 28 after BLI, the primary tumors were resected, and immunohistochemical method was used to aid in the visualization of NEDD9. C, *in vivo* BLI. NOG mice transplanted of PC-14 Luc/Vec or PC-14 Luc/NEDD9 were subjected to BLI procedure on day 28. Ventral and left-lateral (L-Lat) images were obtained after injection of D-luciferin intraperitoneally. Left, representative BLI. Right, the mean signal intensity of ROI was plotted with error bar ($n = 2$). White bar, PC-14 Luc/Vec; black bar, PC-14 Luc/NEDD9. D, expression of transfected NEDD9 in PC-14 cells. Immunoblotting of PC-14 cells stably transfected with BCMG hygro (Vec), BCMG hygro c-myc NEDD9 WT (WT), BCMG hygro c-myc NEDD9 ΔSH3 (ΔSH3), BCMG hygro c-myc NEDD9 ΔC (ΔC). Blotting was conducted with anti-c-myc mAb (9E10).

of 60) of primary human lung adenocarcinoma tissues (Fig. 5A). Overexpression of NEDD9 was associated with increasing invasion into mediastinal (N2) lymph node ($P = 0.01$), pathologic lymphatic invasion ($P = 0.03$), and pathologic venous invasion ($P = 0.03$; Fig. 5B). However, no other statistically significant correlation was found in lung cancer between NEDD9 expression and other clinical parameters, such as age, sex, smoking history, and the extent of primary tumor (Table 1).

With a median follow-up time of 58.5 months (range, 7–91 months), the median RFS was significantly longer in the NEDD9-negative group (not reached) than in the NEDD9-positive group (23 months; $P < 0.001$; Fig. 5C). The HR for RFS was 4.24 [95% confidence interval (CI), 1.93–9.26] in the NEDD9-positive group. The median OS was also significantly longer in the NEDD9-negative group (not reached) than in the NEDD9-positive group (36 months; $P < 0.001$; Fig. 5C).

In univariate Cox analysis, the HR for OS was 5.35 (95% CI, 1.98–14.50) in the NEDD9-positive group. In addition, N2 invasion and pathologic lymphatic invasion were also significant predictors by univariate analysis. In multivariate Cox analysis, NEDD9 expression (HR, 3.88; 95% CI, 1.34–11.23; $P = 0.01$) and pathologic lymphatic invasion (HR,

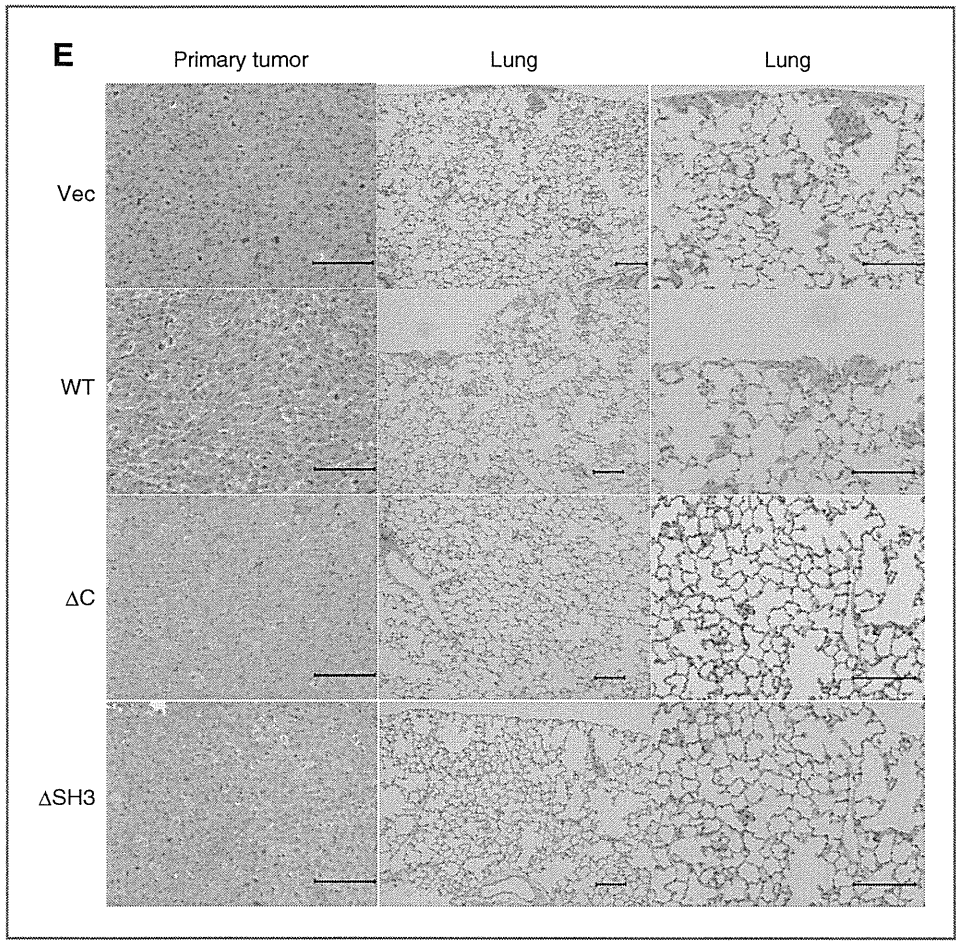

Figure 4. (*Continued*) E, H&E staining of lung tissue from the xenograft-transplanted NOG mice. At necropsy on day 28, the primary tumors and lung tissues were removed from the NOG mice transplanted with each PC-14 transfectant shown in D and stained with H&E. Vec, PC-14 BCMG hygro; WT, PC-14 BCMG hygro c-myc NEDD9 WT; ΔC, PC-14 BCMG hygro c-myc NEDD9 ΔC; and ΔSH3, PC-14 BCMG hygro c-myc NEDD9 ΔSH3. Each scale bar corresponds to 100 μm.

4.94; 95% CI, 1.04–23.5; $P = 0.04$) were independent prognostic variables (summarized in Table 1). Taken together, these results suggest that the expression of NEDD9 closely correlates with venous and lymphatic invasion of cancer cells, and NEDD9 may also be a predictive biomarker for the recurrence and prognosis of human NSCLCs in the clinical setting.

Discussion

In the present study, we showed that tyrosine phosphorylation of NEDD9 was reduced by the inhibition of EGFR in NSCLC cell lines. A constitutively active mutant of EGFR promoted tyrosine phosphorylation of NEDD9 in the absence of integrin signaling. The gene transfer and gene knockdown studies revealed that NEDD9 plays a pivotal role in cell migration and invasion of NSCLC cell line. Overexpression of NEDD9 was shown to promote lung metastasis of an NSCLC cell line in a murine xenograft transplantation model. Finally, the evaluation of the clinical specimens of NSCLCs revealed a strong correlation between NEDD9 expression and RFS or OS, suggesting that NEDD9 is a promising prognostic biomarker in NSCLCs. This is the first study to show the clinical importance of NEDD9 as a prognostic factor as well as the crosstalk between EGFR and NEDD9 signaling pathways in NSCLCs.

Several protein tyrosine kinases (PTK) phosphorylate NEDD9, including FAK (21, 22), RAFTK/Pyk2 (20), Src family PTKs (20, 21), platelet-derived growth factor receptor (PDGFR; ref. 36), Abl (17), and Bcr-Abl (37), many of which are involved in cancer progression and growth. EGFR and PDGFR are RTKs (3) that crosstalk with integrins (8–10, 12), with EGFR physically associating with α5β1 (38) and PDGFR with αvβ3 (39). Engagement of EGFR modulates tyrosine phosphorylation of BCAR1, mediated partly by Src (9), whereas engagement of integrins induces tyrosine phosphorylation of EGFR, mediated by BCAR1 and Src (40, 41). FAK is also a necessary component for EGFR- and PDGFR-induced cell motility (42). These reports suggest that RTKs and integrins form a macromolecular signaling complex at least transiently and have reciprocally compensatory roles in contributing to cell migration and invasion. In this study, we show that NEDD9 may also be an integrator of EGFR and β1-integrin in phosphorylation-dependent signaling, leading to cell migration and invasion of NSCLCs. In this regard, it is possible that other molecules may be associated with EGFR in regulating NEDD9 tyrosine phosphorylation, and additional work is needed to further characterize the signaling complex involving NEDD9, EGFR, and β1-integrins in tumorigenesis and metastasis of NSCLCs.

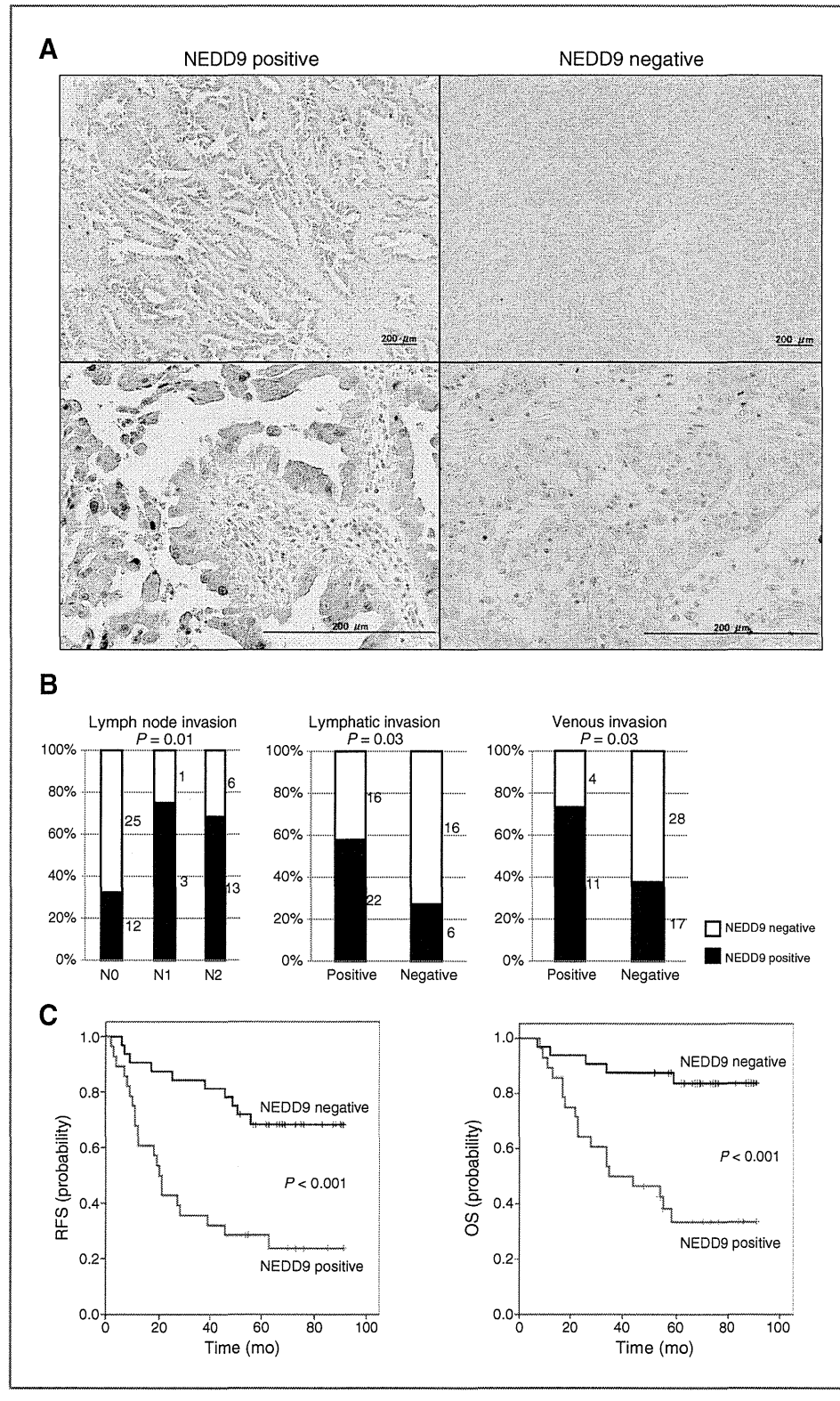

Figure 5. Clinical relevance of NEDD9 expression in NSCLCs. A, immunohistochemical analysis of NEDD9 in primary human lung adenocarcinoma tissues. Top left and bottom left, representative positive staining for NEDD9. Top right and bottom right, representative negative staining for NEDD9. Each scale bar corresponds to 200 μm. B, χ^2 analysis of NEDD9 expression and pathologic invasion of NSCLCs. Left, NEDD9 expression was negative in 68% and positive in 32% in N0, negative in 25% and positive in 75% in N1, negative in 32% and positive in 68% in N2, pathologic node invasion ($P = 0.01$). Middle, NEDD9 expression was negative in 42% and positive in 58% in pathologic lymphatic invasion ($P = 0.03$). Right, NEDD9 expression was negative in 27% and positive in 73% in pathologic venous invasion ($P = 0.03$). C, left, Kaplan–Meier curves for RFS according to NEDD9 expression. Right, Kaplan–Meier curves for OS according to NEDD9 expression.

PC-9 cells used in this study harbors an in-frame deletion in EGFR which causes the receptor to be constitutively activated as a result of structural change proximal to the ATP-binding site (43). These cells and a significant population of NSCLC tumor cells are dependent on the constitutively activated EGFR, thus blockade of the signal by gefitinib results in apoptotic cell death (6, 7). In the context of oncogene involvement in tumor growth, of particular

Table 1. Cox univariate and multivariate analysis of patients with NSCLCs

	RFS		OS	
	HR (95% CI)	*P*	HR (95% CI)	*P*
Univariate analysis				
NEDD9 (positive vs. negative)	4.24 (1.93–9.26)	<0.001	5.35 (1.98–14.50)	0.001
Sex (male vs. female)	1.08 (0.53–2.20)	0.83	1.3 (0.56–3.00)	0.54
Age (>65 y)	1.17 (0.58–2.38)	0.66	1.11 (0.49–2.51)	0.8
Smoking history (smoker vs. non-smoker)	1.19 (0.58–2.39)	0.65	1.25 (0.55–2.84)	0.59
pStage (III vs. I–II)	2.42 (1.20–4.91)	0.01	3.1 (1.35–7.13)	0.01
N1 (positive vs. negative)	1.45 (0.35–6.12)	0.61	1.22 (0.16–9.09)	0.85
N2 (positive vs. negative)	3.9 (1.91–7.97)	<0.001	4.8 (2.05–11.21)	<0.001
Lymphatic invasion (positive vs. negative)	5.83 (2.23–15.28)	<0.001	10.1 (2.36–43.2)	0.002
Venous invasion (positive vs. negative)	1.85 (0.85–4.06)	0.12	2.713 (1.17–6.29)	0.02
Multivariate analysis				
NEDD9 (positive vs. negative)	3.08 (1.37–6.93)	0.006	3.88 (1.34–11.23)	0.01
pStage (III vs. I–II)	0.78 (0.24–2.5)	0.67	1.32 (0.38–4.47)	0.66
N2 (positive vs. negative)	2.54 (0.76–8.46)	0.13	1.84 (0.53–6.39)	0.34
Lymphatic invasion (positive vs. negative)	4.84 (1.52–15.37)	0.008	4.94 (1.04–23.5)	0.04
Venous invasion (positive vs. negative)	0.62 (0.26–1.44)	0.26	0.79 (0.31–1.99)	0.62

interest is that blockade of EGFR signal caused not only dephosphorylation but also a reduction in the protein levels of focal adhesion resident proteins such as BCAR1 and FAK as well as NEDD9. Because these proteins have been reported to incur caspase-induced degradation in apoptosis (44), the results observed in this study may reflect a gefitinib-induced apoptotic process. Supporting this notion, gene transfer of NEDD9 into PC-9 and A549 cells conferred resistance to the chemotherapeutic reagents such as gefitinib, paclitaxel, and cisplatin (Supplementary Figs. S2 and S3). Future in-depth studies will be conducted to expand on these interesting data.

We and others previously reported that NEDD9 phosphorylation contributes to cell migration and invasion (22, 23, 36, 45). We now show the involvement of NEDD9 in EGFR-mediated cell migration and invasion of NSCLCs. Consistent with previous reports, our studies indicated that BCAR1 siRNA also caused significant reduction in EGFR-mediated cell motility of NSCLCs. Another member of Cas family, BCAR1/p130Cas, was independently identified as the primary gene that confers breast cancer cells with resistance to anti-estrogen (46). HER2/neu is a member of the EGFR family and is a notable therapeutic target of breast cancer, similar to EGFR in NSCLCs (47). Interestingly, a double-transgenic mice of MMTV-BCAR1 and MMTV-HER2/neu developed multifocal mammary tumors with a significant shorter latency than the MMTV-HER2/neu transgenic mice (48). Because elevated expression of HER2 accounts for 3% of NSCLC cases, the interaction between HER2 and NEDD9 and the clinical relevance of BCAR1 in NSCLCs remain to be elucidated as a future goal.

Deletion of SH3 domain or SD domain equivalently affected the EGF/integrin-mediated cell motility and invasiveness. Because FAK associates with SH3 domain and Nck or Crk with SD domain of NEDD9 (14, 17), these kinase and adaptor proteins may be critical components of EGF/integrin-induced NEDD9 functions in NSCLCs. Crk forms complex with DOCK180, Nck with WASP and PAK, with both of these complexes relaying signals to the Rho family GTPases Rac and Cdc42, thereby reorganizing actin cytoskeleton (18). On the basis of the results with YDYVHL mutants, upstream Src family PTKs may also contribute to EGF/integrin-mediated NEDD9 function, in accordance with the recently published reports (9, 40, 41). In view of the result with NEDD9 ΔC, serine-rich region is also important for cellular migration elicited by NEDD9. Of interest is that corresponding region of BCAR1 is recently reported to fold as a 4-helix bundle, a protein interaction motif seen in FAK, α-catenin, and vinculin (49).

In the clinical setting, recent studies have indicated that the expression levels of NEDD9 mRNA and protein were elevated in a variety of malignancies such as melanoma (26), glioblastoma (36), breast cancer (27), and that NEDD9 protein is an essential switch for prometastatic behavior of tumor cells. Indeed, some of these studies described NEDD9 as one of the metastatic signature (25, 27). NEDD9 may function in metastasis of colorectal cancer and head and neck squamous cell carcinoma, processes which potentially involve novel upstream molecules such as hypoxia-inducible factor (28), N-terminal truncated carboxypeptidase E splice isoform (29), Wnt (31), and VEGF (50). Our analysis of the clinical records of patients undergoing surgical resection with curative intent of their NSCLCs (with a recurrence rate within 2 years of specimen collection of 43% being similar to the rate reported previously) to evaluate the potential clinical significance of NEDD9 expression in NSCLCs showed a significant correlation between NEDD9 expression and previously

identified pathologic prognostic factors. Expression of NEDD9 was associated with a significant increase in the risk of metastasis and recurrence, with a corresponding decrease in survival and worsened clinical outcome. Multivariate analysis also suggested that NEDD9 expression is an independent predictive factor for the recurrence of NSCLCs. To evaluate the NEDD9 expression in NSCLCs, we set 3 cutoff values (10%, 30%, 50%). Kaplan–Meier curves in the cases with 10% cutoff and 50% cutoff value are shown in Supplementary Fig. S4. When the cutoff value (% positive cells) was 10%, there was no statistically significant difference in OS and RFS. When the cutoff was 50%, the number of positive cases was only 6. When the cutoff was 30%, significant difference was observed in OS and RFS. It should be noted that these data were derived from a retrospective analysis and are likely to suffer from selection bias. Randomized control study or stratified analysis will be necessary in a future study to extend our present findings.

In conclusion, our present work suggests that NEDD9 is a predictive factor for recurrence and prognosis in NSCLCs. Although a variety of gene profiles have been reported to correlate with recurrence of NSCLCs, none has yet been definitely established (51). Because the clinical records evaluated in this study did not contain genetical information on EGFR mutation, KRAS mutation which may affect the sensitivity to gefitinib (52), further comprehensive analysis is necessary in the next step. Optimal strategies to prevent recurrence and metastasis of NSCLCs may need to incorporate NEDD9 expression as one of the promising predictive factors and NEDD9 itself may be a novel therapeutic target for future NSCLC treatment.

Disclosure of Potential Conflicts of Interest

No potential conflicts of interest were disclosed.

Authors' Contributions

Conception and design: S. Kondo, S. Iwata, H. Kawasaki, H. Tanaka, C. Morimoto

Development of methodology: S. Kondo, S. Iwata, T. Yamada, H. Kawasaki

Acquisition of data (provided animals, acquired and managed patients, provided facilities, etc.): S. Kondo, T. Yamada, Y. Inoue, H. Ichihara, Y. Kichikawa, T. Katayose, A. Souta-Kuribara, Y. Hayashi, K. Kamiya

Analysis and interpretation of data (e.g., statistical analysis, biostatistics, computational analysis): S. Kondo, S. Iwata, T. Yamada, Y. Inoue, Y. Kichikawa, H. Yamazaki, H. Kawasaki, N.H. Dang

Writing, review, and/or revision of the manuscript: S. Kondo, S. Iwata, Y. Kichikawa, O. Hosono, H. Kawasaki, N.H. Dang, C. Morimoto

Administrative, technical, or material support (i.e., reporting or organizing data, constructing databases): S. Kondo, T. Yamada, Y. Inoue, H. Ichihara, A. Souta-Kuribara, H. Yamazaki, O. Hosono, M. Sakamoto

Study supervision: S. Iwata, H. Yamazaki, O. Hosono, H. Kawasaki, H. Tanaka, C. Morimoto

Acknowledgments

The authors thank Jun Suzuki and Yukiko Nagafuji for secretarial assistance.

Grant Support

This work was supported by grants-in aid from the Ministry of Education, Science, Sports and Culture (S. Iwata and C. Morimoto), and Ministry of Health, Labor and Welfare, Japan, and by the Program for Promotion of Fundamental Studies in Health Sciences of the National Institute of Biomedical Innovation (C. Morimoto).

The costs of publication of this article were defrayed in part by the payment of page charges. This article must therefore be hereby marked *advertisement* in accordance with 18 U.S.C. Section 1734 solely to indicate this fact.

Received August 23, 2011; revised August 20, 2012; accepted August 28, 2012; published OnlineFirst October 4, 2012.

References

1. Boyle P, Levin B. International Agency for Research on Cancer, World Health Organization. World cancer report 2008. Lyon, France; Geneva, Switzerland: International Agency for Research on Cancer; Distributed by WHO Press; 2008.
2. Winton T, Livingston R, Johnson D, Rigas J, Johnston M, Butts C, et al. Vinorelbine plus cisplatin vs. observation in resected non-small-cell lung cancer. N Engl J Med 2005;352:2589–97.
3. Schlessinger J. Cell signaling by receptor tyrosine kinases. Cell 2000;103:211–25.
4. Arteaga CL. The epidermal growth factor receptor: from mutant oncogene in nonhuman cancers to therapeutic target in human neoplasia. J Clin Oncol 2001;19:32S–40S.
5. Herbst RS, Khuri FR, Fossella FV, Glisson BS, Kies MS, Pisters KM, et al. ZD1839 (Iressa) in non-small-cell lung cancer. Clin Lung Cancer 2001;3:27–32.
6. Lynch TJ, Bell DW, Sordella R, Gurubhagavatula S, Okimoto RA, Brannigan BW, et al. Activating mutations in the epidermal growth factor receptor underlying responsiveness of non-small-cell lung cancer to gefitinib. N Engl J Med 2004;350:2129–39.
7. Paez JG, Janne PA, Lee JC, Tracy S, Greulich H, Gabriel S, et al. EGFR mutations in lung cancer: correlation with clinical response to gefitinib therapy. Science 2004;304:1497–500.
8. Morello V, Cabodi S, Sigismund S, Camacho-Leal MP, Repetto D, Volante M, et al. β1 integrin controls EGFR signaling and tumorigenic properties of lung cancer cells. Oncogene 2011;30:4087–96.
9. Ricono JM, Huang M, Barnes LA, Lau SK, Weis SM, Schlaepfer DD, et al. Specific cross-talk between epidermal growth factor receptor and integrin alphavbeta5 promotes carcinoma cell invasion and metastasis. Cancer Res 2009;69:1383–91.
10. Walker JL, Assoian RK. Integrin-dependent signal transduction regulating cyclin D1 expression and G1 phase cell cycle progression. Cancer Metastasis Rev 2005;24:383–93.
11. Desgrosellier JS, Cheresh DA. Integrins in cancer: biological implications and therapeutic opportunities. Nat Rev Cancer 2010;10:9–22.
12. ffrench-Constant C, Colognato H. Integrins: versatile integrators of extracellular signals. Trends Cell Biol 2004;14:678–86.
13. Nojima Y, Rothstein DM, Sugita K, Schlossman SF, Morimoto C. Ligation of VLA-4 on T cells stimulates tyrosine phosphorylation of a 105-kD protein. J Exp Med 1992;175:1045–53.
14. Minegishi M, Tachibana K, Sato T, Iwata S, Nojima Y, Morimoto C. Structure and function of Cas-L, a 105-kD Crk-associated substrate-related protein that is involved in beta 1 integrin-mediated signaling in lymphocytes. J Exp Med 1996;184:1365–75.
15. Sakai R, Iwamatsu A, Hirano N, Ogawa S, Tanaka T, Mano H, et al. A novel signaling molecule, p130, forms stable complexes *in vivo* with v-Crk and v-Src in a tyrosine phosphorylation-dependent manner. EMBO J 1994;13:3748–56.
16. Kumar S, Tomooka Y, Noda M. Identification of a set of genes with developmentally down-regulated expression in the mouse brain. Biochem Biophys Res Commun 1992;185:1155–61.
17. Law SF, Estojak J, Wang B, Mysliwiec T, Kruh G, Golemis EA. Human enhancer of filamentation 1, a novel p130cas-like docking protein, associates with focal adhesion kinase and induces pseudohyphal growth in *Saccharomyces cerevisiae*. Mol Cell Biol 1996;16:3327–37.

18. O'Neill GM, Seo S, Serebriiskii IG, Lessin SR, Golemis EA. A new central scaffold for metastasis: parsing HEF1/Cas-L/NEDD9. Cancer Res 2007;67:8975–9.
19. Ohashi Y, Tachibana K, Kamiguchi K, Fujita H, Morimoto C. T cell receptor-mediated tyrosine phosphorylation of Cas-L, a 105-kDa Crk-associated substrate-related protein, and its association of Crk and C3G. J Biol Chem 1998;273:6446–51.
20. Manie SN, Beck AR, Astier A, Law SF, Canty T, Hirai H, et al. Involvement of p130(Cas) and p105(HEF1), a novel Cas-like docking protein, in a cytoskeleton-dependent signaling pathway initiated by ligation of integrin or antigen receptor on human B cells. J Biol Chem 1997; 272:4230–6.
21. Tachibana K, Urano T, Fujita H, Ohashi Y, Kamiguchi K, Iwata S, et al. Tyrosine phosphorylation of Crk-associated substrates by focal adhesion kinase. A putative mechanism for the integrin-mediated tyrosine phosphorylation of Crk-associated substrates. J Biol Chem 1997; 272:29083–90.
22. van Seventer GA, Salmen HJ, Law SF, O'Neill GM, Mullen MM, Franz AM, et al. Focal adhesion kinase regulates beta1 integrin-dependent T cell migration through an HEF1 effector pathway. Eur J Immunol 2001;31:1417–27.
23. Ohashi Y, Iwata S, Kamiguchi K, Morimoto C. Tyrosine phosphorylation of Crk-associated substrate lymphocyte-type is a critical element in TCR- and beta 1 integrin-induced T lymphocyte migration. J Immunol 1999;163:3727–34.
24. Iwata S, Souta-Kuribara A, Yamakawa A, Sasaki T, Shimizu T, Hosono O, et al. HTLV-I Tax induces and associates with Crk-associated substrate lymphocyte type (Cas-L). Oncogene 2005;24:1262–71.
25. Ji H, Ramsey MR, Hayes DN, Fan C, McNamara K, Kozlowski P, et al. LKB1 modulates lung cancer differentiation and metastasis. Nature 2007;448:807–10.
26. Kim M, Gans JD, Nogueira C, Wang A, Paik JH, Feng B, et al. Comparative oncogenomics identifies NEDD9 as a melanoma metastasis gene. Cell 2006;125:1269–81.
27. Minn AJ, Gupta GP, Siegel PM, Bos PD, Shu W, Giri DD, et al. Genes that mediate breast cancer metastasis to lung. Nature 2005;436: 518–24.
28. Kim SH, Xia D, Kim SW, Holla V, Menter DG, Dubois RN. Human enhancer of filamentation 1 Is a mediator of hypoxia-inducible factor-1alpha-mediated migration in colorectal carcinoma cells. Cancer Res 2010;70:4054–63.
29. Lee TK, Murthy SR, Cawley NX, Dhanvantari S, Hewitt SM, Lou H, et al. An N-terminal truncated carboxypeptidase E splice isoform induces tumor growth and is a biomarker for predicting future metastasis in human cancers. J Clin Invest 2011;121:880–92.
30. Li Y, Bavarva JH, Wang Z, Guo J, Qian C, Thibodeau SN, et al. HEF1, a novel target of Wnt signaling, promotes colonic cell migration and cancer progression. Oncogene 2011;30:2633–43.
31. Xia D, Holla VR, Wang D, Menter DG, DuBois RN. HEF1 is a crucial mediator of the proliferative effects of prostaglandin E(2) on colon cancer cells. Cancer Research 2010;70:824–31.
32. Koizumi F, Shimoyama T, Taguchi F, Saijo N, Nishio K. Establishment of a human non-small cell lung cancer cell line resistant to gefitinib. Int J Cancer 2005;116:36–44.
33. Greulich H, Chen TH, Feng W, Janne PA, Alvarez JV, Zappaterra M, et al. Oncogenic transformation by inhibitor-sensitive and -resistant EGFR mutants. PLoS Med 2005;2:e313.
34. Inoue Y, Tojo A, Sekine R, Soda Y, Kobayashi S, Nomura A, et al. *In vitro* validation of bioluminescent monitoring of disease progression and therapeutic response in leukaemia model animals. Eur J Nucl Med Mol Imaging 2006;33:557–65.
35. Ito M, Hiramatsu H, Kobayashi K, Suzue K, Kawahata M, Hioki K, et al. NOD/SCID/gamma(c)(null) mouse: an excellent recipient mouse model for engraftment of human cells. Blood 2002; 100:3175–82.
36. Natarajan M, Stewart JE, Golemis EA, Pugacheva EN, Alexandropoulos K, Cox BD, et al. HEF1 is a necessary and specific downstream effector of FAK that promotes the migration of glioblastoma cells. Oncogene 2006;25:1721–32.
37. de Jong R, van Wijk A, Haataja L, Heisterkamp N, Groffen J. BCR/ABL-induced leukemogenesis causes phosphorylation of Hef1 and its association with Crkl. J Biol Chem 1997;272:32649–55.
38. Lee JW, Juliano RL. The alpha5beta1 integrin selectively enhances epidermal growth factor signaling to the phosphatidylinositol-3-kinase/Akt pathway in intestinal epithelial cells. Biochim Biophys Acta 2002;1542:23–31.
39. Ding Q, Stewart J Jr, Olman MA, Klobe MR, Gladson CL. The pattern of enhancement of Src kinase activity on platelet-derived growth factor stimulation of glioblastoma cells is affected by the integrin engaged. J Biol Chem 2003;278:39882–91.
40. Moro L, Dolce L, Cabodi S, Bergatto E, Boeri Erba E, Smeriglio M, et al. Integrin-induced epidermal growth factor (EGF) receptor activation requires c-Src and p130Cas and leads to phosphorylation of specific EGF receptor tyrosines. J Biol Chem 2002;277: 9405–14.
41. Leung EL, Tam IY, Tin VP, Chua DT, Sihoe AD, Cheng LC, et al. SRC promotes survival and invasion of lung cancers with epidermal growth factor receptor abnormalities and is a potential candidate for molecular-targeted therapy. Mol Cancer Res 2009;7: 923–32.
42. Sieg DJ, Hauck CR, Ilic D, Klingbeil CK, Schaefer E, Damsky CH, et al. FAK integrates growth-factor and integrin signals to promote cell migration. Nat Cell Biol 2000;2:249–56.
43. Sakai K, Arao T, Shimoyama T, Murofushi K, Sekijima M, Kaji N, et al. Dimerization and the signal transduction pathway of a small in-frame deletion in the epidermal growth factor receptor. FASEB J 2006; 20:311–3.
44. Law SF, O'Neill GM, Fashena SJ, Einarson MB, Golemis EA. The docking protein HEF1 is an apoptotic mediator at focal adhesion sites. Mol Cell Biol 2000;20:5184–95.
45. Seo S, Asai T, Saito T, Suzuki T, Morishita Y, Nakamoto T, et al. Crk-associated substrate lymphocyte type is required for lymphocyte trafficking and marginal zone B cell maintenance. J Immunol 2005;175:3492–501.
46. Brinkman A, van der Flier S, Kok EM, Dorssers LC. BCAR1, a human homologue of the adapter protein p130Cas, and antiestrogen resistance in breast cancer cells. J Natl Cancer Inst 2000;92:112–20.
47. Zhou BP, Hung MC. Dysregulation of cellular signaling by HER2/neu in breast cancer. Semin Oncol 2003;30:38–48.
48. Cabodi S, Tinnirello A, Di Stefano P, Bisaro B, Ambrosino E, Castellano I, et al. p130Cas as a new regulator of mammary epithelial cell proliferation, survival, and HER2-neu oncogene-dependent breast tumorigenesis. Cancer Res 2006;66:4672–80.
49. Briknarova K, Nasertorabi F, Havert ML, Eggleston E, Hoyt DW, Li C, et al. The serine-rich domain from Crk-associated substrate (p130cas) is a four-helix bundle. J Biol Chem 2005;280:21908–14.
50. Lucas JT Jr, Salimath BP, Slomiany MG, Rosenzweig SA. Regulation of invasive behavior by vascular endothelial growth factor is HEF1-dependent. Oncogene 2010;29:4449–59.
51. Potti A, Mukherjee S, Petersen R, Dressman HK, Bild A, Koontz J, et al. A genomic strategy to refine prognosis in early-stage non-small-cell lung cancer. N Engl J Med 2006;355:570–80.
52. Hirsch FR, Varella-Garcia M, Bunn PA Jr, Franklin WA, Dziadziuszko R, Thatcher N, et al. Molecular predictors of outcome with gefitinib in a phase III placebo-controlled study in advanced non-small-cell lung cancer. J Clin Oncol 2006;24:5034–42.

CORRESPONDENCE

Extrapulmonary small cell carcinoma mimicking malignant pleural mesothelioma

We report a case with a history of occupational asbestos exposure in which malignant pleural mesothelioma (MPM) was suspected clinically and diagnosed postmortem as pleural involvement of extrapulmonary small cell carcinoma (SCC). An 85-year-old man with a 65 pack-year history of smoking was referred to our hospital in June 2011. The patient had been exposed to asbestos in the iron production industry over the course of 30 years, and an irregular thickening of the right pleura was observed on chest CT at a medical check-up. The patient had a history of chronic hepatitis C and had been undergone transurethral resection for urothelial bladder cancer five times since 2006. Chest CT revealed neoplastic thickening of the right pleura, which had grown over 6 months (figure 1). The CT scan demonstrated bilateral pleural plaques, but no mass-like lesion in other organs, including the lungs, or mediastinal lymphadenopathy. The patient was suspected as having MPM and scheduled for thoracoscopic pleural biopsy, but his general condition worsened rapidly and he died due to pneumonia in August 2011. Autopsy revealed multiple tumours on the right chest wall, as well as multiple tumours in the bilateral lung, liver, pancreas and prostate, which were not detected in the CT scan in July 2011. H&E staining revealed similar histology for the tumours on the lung and pleura; the tumour cells were small with an increased cytoplasm to nucleus ratio. Immunohistochemical analysis revealed that these tumour cells were positive for CD56 (figure 2) but negative for chromogranin, synaptophysin, thyroid transcription factor (TTF)-1 and calretinin. Based on these findings, the patient was diagnosed with SCC.

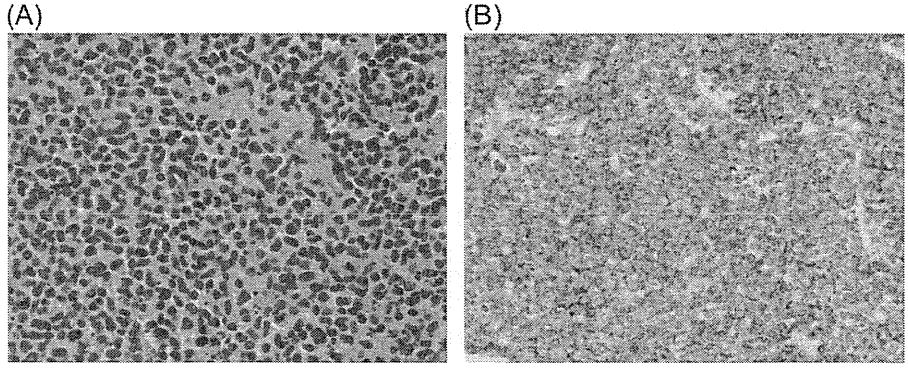

Figure 2 Pathological findings for the pleural tumour. (A) H&E staining revealed that the tumour cells were small with an increased cytoplasm to nucleus ratio. (B) Immunohistochemical analysis revealed that these tumour cells were positive for CD56.

Figure 3 The small cell carcinoma component was detected in the resected bladder specimen in 2006.

In addition, transitional cell carcinoma was detected in the bladder by postmortem microscopic analysis, suggesting residual or recurrent bladder cancer. The patient was considered as having extrapulmonary SCC because no mass-like lesion was found in the lung antemortem, and detailed pathological examination revealed that the SCC component was detected in the bladder specimen resected in 2006 (figure 3). The bladder specimen was partially positive for CD56, and negative for chromogranin and synaptophysin. Finally, the patient was diagnosed with recurrence of SCC originating in the bladder.

The current case was clinically suspected as MPM because the patient had a history of occupational asbestos exposure and the CT scan demonstrated neoplastic pleural thickening. Autopsy gave the postmortem diagnosis of SCC. We think that the SCC in the current case was

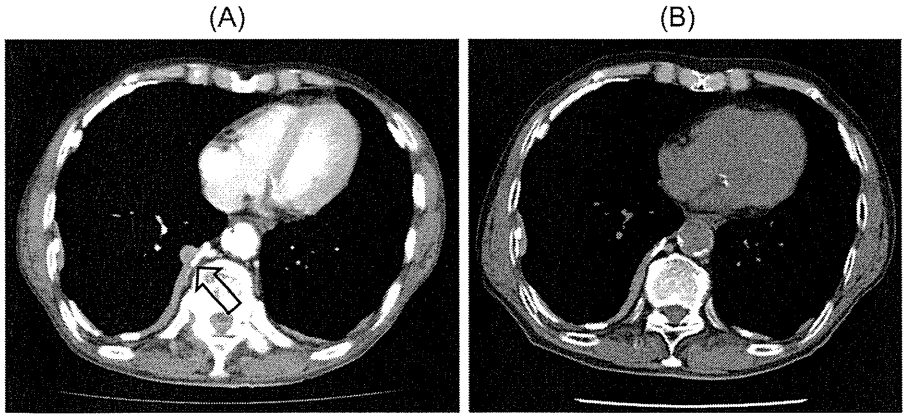

Figure 1 (A) Chest CT at initial presentation revealed neoplastic thickening of the right pleura. (B) The neoplastic lesion was not detected in the CT scan 6 months prior.

extrapulmonary in origin based on the following. First, neoplastic pleural thickening was the initial finding without any evidence of the lesions in other organs, including the lung. Second, the cancer cells were TTF-1-negative. TTF-1 has been reported to be present in pulmonary SCC, but not in extrapulmonary SCC, though there is another report that a large number of extrapulmonary SCC express TTF-1.[1]

Extrapulmonary SCC is uncommon but occurs at various sites.[2] In the current case, postmortem macroscopic analysis revealed tumours in the lung, pleura, liver and pancreas. At the time of the autopsy, we thought that the pleura was the origin because the neoplastic pleural thickening was the initial clinical finding, though primary SCC of the pleura is quite rare and only a few cases have been reported.[3 4] Ultimately, we determined that the SCC in the current case was a recurrence of SCC of the bladder because detailed pathological examination of the bladder resected in 2006 revealed the SCC component. SCC of the bladder is also quite rare, accounting for less than 1% of all bladder tumours[5] and often coexists with another tumour component, such as urothelial carcinoma,[6] as in the present case.

In patients with irregular pleural thickening, especially those with a history of asbestos exposure, MPM is the most common neoplasm. However, extrapulmonary SCC should be noted as a differential diagnosis.

Kaoru Noguchi,[1] Nobukazu Fujimoto,[1] Michiko Asano,[1] Yasuko Fuchimoto,[1] Katsuichiro Ono,[1] Shinji Ozaki,[1] Katsuyuki Hotta,[2] Katsuya Kato,[3] Hiroko Toda,[4] Koji Taguchi,[5] Takumi Kishimoto[1]

[1]Department of Respiratory Medicine, Okayama Rosai Hospital, Okayama, Japan
[2]Department of Respiratory Medicine, Okayama University Hospital, Okayama, Japan
[3]Department of Radiology, Okayama University Hospital, Okayama, Japan
[4]Department of Pathology, Okayama University Hospital, Okayama, Japan
[5]Department of Pathology, Okayama Rosai Hospital, Okayama, Japan

Correspondence to Dr Nobukazu Fujimoto, Department of Respiratory Medicine, Okayama Rosai Hospital, 1-10-25 Chikkomidorimachi, Minamiku, Okayama 7028055, Japan; nfuji@okayamaH.rofuku.go.jp

Contributors KN treated the patient and drafted the paper. NF treated the patient and drafted and revised the paper. MA, YF, KO and SO contributed to the data monitoring and drafted and revised the paper. KH first found the CT finding of the patient and analysed the patient data. KK analysed the radiological images of the patients. HT and KT contributed to the pathological examination of the patients. TK finally approved the work to be published.

Funding This research is a part of the research and development and the dissemination projects related to the 13 fields of occupational injuries and illnesses of the Japan Labour Health and Welfare Organization.

Competing interests None.

Patient consent Obtained.

Provenance and peer review Not commissioned; externally peer reviewed.

To cite Noguchi K, Fujimoto N, Asano M, *et al*. *J Clin Pathol* Published Online First: [*please include* Day Month Year] doi:10.1136/jclinpath-2012-201401

J Clin Pathol 2013;**0**:1–2.
doi:10.1136/jclinpath-2012-201401

REFERENCES

1 Cheuk W, Kwan MY, Suster S, *et al*. Immunostaining for thyroid transcription factor 1 and cytokeratin 20 aids the distinction of small cell carcinoma from Merkel cell carcinoma, but not pulmonary from extrapulmonary small cell carcinomas. *Arch Pathol Lab Med* 2001;125:228–31.
2 Ibrahim NB, Briggs JC, Corbishley CM. Extrapulmonary oat cell carcinoma. *Cancer* 1984;54:1645–61.
3 van der Heijden HF, Heijdra YF, Bulten J, *et al*. Pleural small cell carcinoma in pre-existent asbestos related pleural disease. *Lung Cancer* 2002;35:91–4.
4 Schinkewitch P, Gasser B, Wihlm JM, *et al*. Small cell carcinoma of the pleura. A case report. *Lung Cancer* 1996;16:87–94.
5 Oderda M, Ruoppolo M, Marson F, *et al*. Pathological features and adverse prognosis of a contemporary series of neuroendocrine bladder tumours. *Urol Int* 2011;86:185–90.
6 Cheng L, Pan CX, Yang XJ, *et al*. Small cell carcinoma of the urinary bladder: a clinicopathologic analysis of 64 patients. *Cancer* 2004;101:957–62.

Carcinogenesis vol.33 no.7 pp.1277–1285, 2012
doi:10.1093/carcin/bgs154
Advance Access publication April 24, 2012

Integrated analysis of genetic and epigenetic alterations reveals CpG island methylator phenotype associated with distinct clinical characters of lung adenocarcinoma

Keiko Shinjo[1,2], Yasuyuki Okamoto[1], Byonggu An[1], Toshihiko Yokoyama[3], Ichiro Takeuchi[4], Makiko Fujii[1], Hirotaka Osada[1,2], Noriyasu Usami[5], Yoshinori Hasegawa[3], Hidemi Ito[6], Toyoaki Hida[7], Nobukazu Fujimoto[8], Takumi Kishimoto[8], Yoshitaka Sekido[1,2] and Yutaka Kondo[1,9,*]

[1]Division of Molecular Oncology, Aichi Cancer Center Research Institute, 1-1 Kanokoden, Chikusa-ku, Nagoya 464-8681, Japan, [2]Department of Cancer Genetics, [3]Department of Respiratory Medicine, Nagoya University Graduate School of Medicine, Nagoya, Japan, [4]Graduate School of Engineering, Nagoya Institute of Technology, Nagoya, Japan, [5]Division of General Thoracic Surgery, Nagoya University Graduate School of Medicine, Nagoya, Japan, [6]Division of Epidemiology and Prevention, Aichi Cancer Center Research Institute, Nagoya, Japan, [7]Department of Thoracic Oncology, Aichi Cancer Center Hospital, Nagoya, Japan, [8]Department of Respiratory Medicine, Okayama Rosai Hospital, Okayama, Japan and [9]Precursory Research for Embryonic Science and Technology (PRESTO), Japan Science and Technology Agency, Saitama, Japan

*To whom correspondence should be addressed. Tel: +81 52 764 2994;
Fax: +81 52 764 2994;
Email: ykondo@aichi-cc.jp

DNA methylation affects the aggressiveness of human malignancies. Cancers with CpG island methylator phenotype (CIMP), a distinct group with extensive DNA methylation, show characteristic features in several types of tumors. In this study, we initially defined the existence of CIMP in 41 lung adenocarcinomas (AdCas) through genome-wide DNA methylation microarray analysis. DNA methylation status of six CIMP markers newly identified by microarray analysis was further estimated in a total of 128 AdCas by bisulfite pyrosequencing analysis, which revealed that 10 (7.8%), 40 (31.3%) and 78 (60.9%) cases were classified as CIMP-high (CIMP-H), CIMP-low and CIMP-negative (CIMP-N), respectively. Notably, CIMP-H AdCas were strongly associated with wild-type epidermal growth factor receptor (*EGFR*), males and heavy smokers ($P = 0.0089$, $P = 0.0047$ and $P = 0.0036$, respectively). In addition, CIMP-H was significantly associated with worse prognosis; especially among male smokers, CIMP-H was an independent prognostic factor (hazard ratio 1.7617, 95% confidence interval 1.0030–2.9550, $P = 0.0489$). Compellingly, the existence of CIMP in AdCas was supported by the available public datasets, such as data from the Cancer Genome Atlas. Intriguingly, analysis of AdCa cell lines revealed that CIMP-positive AdCa cell lines were more sensitive to a DNA methylation inhibitor than CIMP-N ones regardless of *EGFR* mutation status. Our data demonstrate that CIMP in AdCas appears to be a unique subgroup that has distinct clinical traits from other AdCas. CIMP classification using our six-marker panel has implications for personalized medical strategies for lung cancer patients; in particular, DNA methylation inhibitor might be of therapeutic benefit to patients with CIMP-positive tumors.

Introduction

Lung cancer is the leading cause of human cancer death worldwide (1). Recent targeted therapies have improved the survival of patients with certain types of lung cancer, especially adenocarcinoma (AdCa), a common type of non-small cell lung cancer. AdCas with epidermal growth factor receptor (*EGFR*) mutation benefit particularly from EGFR tyrosine kinase inhibitors (TKIs) (2), whereas those harboring *EML4–ALK* fusion are highly sensitive to anaplastic lymphoma kinase (ALK) inhibitors (3). Despite these recent advances in targeted therapy for AdCas, a considerable number of patients with lung cancer still suffer from recurrence of disease. AdCas without such mutations are generally less sensitive to these targeted therapies than tumors with mutations. Given the evidence that the frequency of *EGFR* mutations account for up to 30% of AdCas, and even *EML4–ALK* fusions are found in AdCas albeit at a lower frequency, elucidating the underlying mechanisms other than such gene alterations in lung carcinogenesis is desirable to facilitate the development of new strategies for lung cancer treatment.

Studies have shown that in addition to genetic alterations, accumulation of epigenetic alterations play an important role in tumorigenesis of lung cancer (4). DNA methylation, an important epigenetic factor, affects the chromatin structure and is closely associated with gene regulation (5). Simultaneous dysregulation of multiple genes, including those involved in cell cycle, cell growth, cell death or cell adhesion, by DNA methylation may be a strong driving force to undergo transformation, sometimes in correlation with potentiated aggressiveness of the tumors (6).

Recent studies in colon cancer have shown that a subset of tumors suffer from a remarkably high rate of aberrant promoter DNA methylation at a large number of loci, referred to as CpG island methylator phenotype (CIMP) (7). CIMP tumors in colon exhibit distinct genetic and clinical features, such as high rates of *BRAF* and *KRAS* mutations, low frequency of *TP53* mutation, specific histology, proximal location and characteristic clinical outcome, suggesting that CIMP-related cancers may proceed through a unique pathway (8). In lung cancer, some studies have shown the existence of a subgroup of tumors with the characteristic methylation status of CIMP (9–13). However, in comparison with the considerable research of CIMP markers performed in colon cancers (7,14–16), no studies have assessed which DNA methylation markers can predict the most extensively methylated subgroups (i.e. CIMP) in lung AdCas due to the lack of accompanied genome-wide DNA methylation analysis in multiple samples. Since different panels of markers may lead to different classification of lung cancer (9,11), it is important to define markers that can accurately identify CIMP.

To examine whether CIMP exists as a characteristic subgroup in AdCas, we initially performed global screening for genes with aberrant DNA hypermethylation by the methylated CpG island amplification microarray (MCAM) analysis, which provides reproducible results with a high validation rate (16–20). Using the six CIMP markers newly identified by MCAM analysis, we characterized a distinct subgroup of AdCas exhibiting CIMP. In addition, several AdCa cell lines with different CIMP status were treated with a DNA methylation inhibitor, and the relationship between DNA methylation status and drug sensitivity was assessed. Our data provide evidence for a new strategy for lung cancer treatment.

Abbreviations: AdCa, adenocarcinoma; CIMP, CpG island methylator phenotype; CIMP-H, CIMP-high; CIMP-L, CIMP-low; CIMP-N, CIMP-negative; EGFR, epidermal growth factor receptor; MCAM, methylated CpG island amplification microarray; TCGA, the cancer genome atlas; TKI, tyrosine kinase inhibitor;

Materials and methods

Cell lines

A549 was purchased from the American Type Culture Collection (Rockville, MD) and PC9 was purchased from Immuno-Biological Laboratories (Fujioka, Gunma, Japan). NCI-H23, NCI-H358, NCI-H920, NCI-H2009, NCI-H1573, NCI-H1650 and HCC4011 were kind gifts from Dr Adi F. Gazdar (University of Texas Southwestern Medical Center, Dallas, TX) and Dr Mitsuo Sato (Nagoya University Graduate School of Medicine, Nagoya, Japan). Y-ML13 (ML13) and ACC-H1 (H1) were established in our institute. All cell lines were maintained in RPMI-1640 medium (Sigma–Aldrich, St Louis, MO) supplemented with 10%

fetal bovine serum (Invitrogen, Carlsbad, CA) and antibiotic–antimycotic reagent (Invitrogen) at 37°C in a humidified incubator with 5% CO_2.

5-Aza-dC treatment of cells

Cells were treated with 50 nM–1 μM 5-aza-2′-deoxycytidine (5-Aza-dC; Sigma–Aldrich) as described previously (17) or the TKI AG1478 (Calbiochem, San Diego, CA) for 72 h. DNA was extracted on the seventh day following treatment. Changes in proliferation were determined by using the TetraColor ONE (Seikagaku, Tokyo, Japan) system, containing 2-(2-methoxy-4-nitrophenyl)-3-(4-nitrophenyl)-5-(2,4-disulfophenyl)-2H-tetrazolium, monosodium salt and 1-methoxy-5-methylphenazinium methylsulfate as the electron carrier. After 1 h incubation at 37°C, absorbance was read at 450 nm with a multiplate reader. Growth inhibition was expressed as a mean ratio of absorbance reading from treated versus untreated cells. Cell numbers were also counted under a light microscope at the same time point.

Tissue samples

We collected 128 AdCa samples and 26 normal lung tissues from patients who underwent surgical resection at the Aichi Cancer Center Central Hospital, Okayama Rosai Hospital, Nagoya University Hospital and its affiliated hospitals in Japan, in accordance with the institutional policy. Samples and clinical data were collected after appropriate institutional review board approval was received and written informed consent had been obtained from all the patients. Histological and cytological examination of normal lung tissues, which were obtained from the lung cancer patients, revealed no remarkable findings as malignant tissues. In the normal tissues, no aberrant methylation was detected in 10 genes by pyrosequencing analysis (Supplementary Table 1, available at *Carcinogenesis* Online). A sample size of 124 patients was calculated to be sufficient to provide a survival rate difference of 25% with a significance level of 0.05 and power of 80%, when the frequency of CIMP-AdCa was estimated to be ~20% as is observed in colorectal cancer (8); therefore, we collected 128 AdCas to analyze the significance of CIMP (Table I).

DNA preparation

Genomic DNA was extracted using a standard phenol–chloroform method. Fully methylated DNA was prepared by treating genomic DNA with *Sss*I methylase (New England Biolabs, Ipswich, MA), and unmethylated DNA was prepared by treating genomic DNA with phi29 DNA polymerase (GenomiPhi DNA Amplification Kit; Amersham Biosciences, Uppsala, Sweden) according to the manufacturers' protocol.

DNA methylation analysis

We performed bisulfite treatment as described previously (21,22).The DNA methylation levels were measured using pyrosequencing technology (Pyrosequencing AB, Uppsala, Sweden). Primer sequences and polymerase chain reaction conditions are shown in Supplementary Table 2, available at *Carcinogenesis* Online. All the primers were designed to examine the methylation status of CpGs within 0.5 kb of the transcription start site. A methylation level >15% was considered methylation positive since lower values could not be easily distinguished from background (17–20).

Methylated CpG island amplification microarray

For MCAM analysis, we randomly selected 41 cases from the 128 AdCas without any bias (average age was 61.9 years, ranging from 36 to 83 years old; Table I). A detailed protocol of MCA has been described previously (16–20). Briefly, amplicons from individual AdCas were labeled with Cy5 dye and cohybridized against amplicons from normal controls labeled with Cy3 dye on 15 K custom-promoter microarrays from Agilent Technologies (G4497A; Agilent Technologies, Santa Clara, CA) containing 6157 unique genes, which we had initially validated in a previous study (17). A Cy5/Cy3 signal in excess of 2.0 in MCAM was considered methylation positive (17–19). Comparison of the MCAM signal ratio (Cy5/Cy3 > 2.0 or Cy5/Cy5 ≤ 2.0) with the methylation status (positive or negative) from the pyrosequencing analysis showed a good concordance between the two analyses (sensitivity, 68.0% and specificity, 88.7%; Supplementary Table 3, available at *Carcinogenesis* Online).

Hierarchical clustering analysis

Cluster analysis was performed using an agglomerative hierarchical clustering algorithm (18,23). For specimen clustering, pairwise similarity measures among specimens were calculated using the Cluster 3.0 software (http://rana.lbl.gov/EisenSoftware.htm) or Minitab 15 statistical software (http://www.minitab.com), based on the DNA methylation intensity measurements

Table I. Clinical and molecular features according to the CIMP status

	All cases (%)	CIMP-N (%)	CIMP-L (%)	CIMP-H (%)	*P* value
Cases	128 (100)	78 (60.9)	40 (31.3)	10 (7.8)	
Age (mean ± SD)	64.7 ± 9.8	63.9 ± 10.0	66.4 ± 9.8	63.8 ± 7.0	0.4043
Gender					
Male	71 (55.5)	35 (44.9)	27 (67.5)	9 (90.0)	0.0047
Female	57 (44.5)	43 (55.1)	13 (32.5)	1 (10.0)	
Stage[a]					
I	75 (59.5)	51 (67.1)	21 (52.5)	3 (30.0)	0.2259
II	19 (15.1)	7 (9.2)	8 (20.0)	3 (30.0)	
III	29 (23.0)	16 (21.1)	10 (25.0)	4 (40.0)	
IV	3 (2.4)	2 (2.6)	1 (2.5)	0 (0)	
Smoking status					
Heavy smoker	41 (32.3)	21 (27.6)	12 (30.8)	8 (80.0)	0.0036
Light smoker	29 (22.8)	15 (19.7)	13 (33.3)	1 (10.0)	
Never-smoker	57 (44.9)	42 (55.3)	14 (35.9)	1 (10.0)	
Differentiation[a]					
Well	15 (17.4)	11 (21.2)	3 (10.7)	1 (16.7)	0.3552
Moderate	55 (64.0)	30 (57.6)	22 (78.6)	3 (50.0)	
Poorly	16 (18.6)	11 (21.2)	3 (10.7)	2 (33.3)	
Recurrence[a]					
(−)	41 (42.3)	27 (43.5)	14 (46.7)	0 (0)	0.1394
(+)	56 (57.7)	35 (56.5)	16 (53.3)	5 (100)	
EGFR mutation					
(−)	80 (62.5)	42 (53.8)	28 (70.0)	10 (100)	0.0089
(+)	48 (37.5)	36 (46.2)	12 (30.0)	0 (0)	
KRAS mutation					
(−)	118 (92.2)	74 (94.9)	36 (90.0)	8 (80.0)	0.2113
(+)	10 (7.8)	4 (5.1)	4 (10.0)	2 (20.0)	
p53 mutation[a]					
(−)	89 (69.5)	57 (74.0)	28 (73.7)	4 (40.0)	0.16
(+)	35 (27.3)	20 (26.0)	10 (26.3)	5 (50.0)	
BRAF mutation					
(−)	86 (100)	56 (100)	23 (100)	7 (100)	NA
(+)	0 (0)	0 (0)	0 (0)	0 (0)	

[a]Data were not available in some cases. Recurrence was observed within 5 years after surgery.

across all genes. *K*-means consensus clustering was performed with the R statistical package. A dendrogram and heat map were constructed using either TreeView (http://rana.lbl.gov/EisenSoftware.htm) or R statistical computing environment (http://cran.r-project.org).

Nearest neighbor classification

Using the DNA methylation status of six CIMP markers (positive or negative by pyrosequencing analysis), nearest neighbor classification was employed to classify the validation set consisting of 87 independent AdCas (24). In this analysis, each validation case was classified into one of the three clusters identified in the training set. The number of nearest neighbors was set as $k = 4$ because the smallest cluster (cluster 1) was consisted of four cases. The analysis was conducted using R statistical computing environment (http://cran.r-project.org).

Mutation analysis

Mutations in *KRAS* (codons 12 and 13) were analyzed by direct sequencing and the pyrosequencing method (25,26). *EGFR* mutations (exons 18–21) and *TP53* mutations (exons 5–8) were examined using direct sequencing (19,25). Mutation of *BRAF* (codon 600) was determined by the pyrosequencing method as previously reported (27). The polymerase chain reaction primer sequences used are listed in Supplementary Table 2, available at *Carcinogenesis* Online.

The Cancer Genome Atlas data

We obtained the methylation data of AdCa samples from the The Cancer Genome Atlas data (TCGA) web site (http://tcga-data.nci.nih.gov/tcga/tcgaHome2.jsp), and data of 85 AdCa samples (batches 34 and 37) were included in the analysis, which was conducted using the Illumina Infinium Human DNA Methylation 27 platform. The 3833 most variant probes from 27 578 CpG dinucleotides were used for further analysis, and a β value > 0.4 was considered as methylation positive.

Statistical analysis for clinical features

All statistical analyses were performed using the JMP statistical software version 5.1 (SAS Institute, Cary, NC). Fisher's exact test was used to determine non-random associations between two categorical variables. Kruskal–Wallis analysis was used to evaluate the extent of differences among more than three groups. All reported *P* values are two sided, with $P < 0.05$ taken as statistically significant. Patients were followed until incidence of death or until October 2010, whichever came first. Survival information was available for 118 of the 128 cases. Overall survival was calculated from the date of surgery until the date of death or the date the patient was last known to be alive (censored). The median follow-up time was 42.5 months. Overall survival curves were generated via the Kaplan–Meier method, and the log-rank test was used for statistical analysis. A multivariate analysis using the Cox proportional hazards model was performed to estimate the hazard ratio. All variables for the multivariate analysis were categorical variables (age, stage and CIMP status).

Results

Identification of a distinct subgroup with characteristic DNA methylation profiling in AdCas

First, we evaluated the genome-wide DNA methylation status in a training set of 41 AdCas using MCAM analysis (18–20). Among 6157 genes on the microarray, we selected 1156 genes that are commonly methylated across >10% of AdCas and performed consensus average linkage hierarchical clustering analysis (28). In terms of DNA methylation, AdCas could be divided into three clusters, with clustering stability increasing for $k = 2$ to $k = 3$ but not for more than $k = 3$ (Figure 1A, Supplementary Figure 1, available at *Carcinogenesis* Online). Intriguingly, all four cases in cluster 1 stably fell into the same cluster regardless of *k* values (2–5), whereas 12 cases (92%) and 24 cases (96%) fell into clusters 2 and 3, respectively, indicating a high similarity of their methylation profile among each of the three-cluster member. The number of DNA methylated genes showed bimodal distribution in AdCas; DNA methylation was highly accumulated in two AdCas, both of which fell into cluster 1# (Figure 1B). Consistently, a majority of the genes were commonly methylated across more than half of the AdCas in cluster 1, whereas common methylation targets were detected in ≤50% of the AdCas in clusters 2 and 3 ($P < 0.001$, Figure 1C). In addition, the average number of methylated genes was 766.8 ± 70.4, 485.7 ± 40.6 and 319.2 ± 28.1 in clusters 1, 2 and 3 (k=3), respectively ($P < 0.001$) (Figure 1D). These observations indicated that extensively methylated AdCas exist, which appear to be characterized by correlated CpG island DNA methylation of a subset of genes in a subset of tumors, whereas AdCas with less extensive DNA methylation or with rare DNA methylation were classified into discrete subgroups (7,14–16).

Identification of CIMP markers in AdCas

MCAM analysis suggested the existence of a distinct subgroup with extensive DNA methylation in AdCas. Because CIMP status is closely associated with clinical outcome in forming a distinct subgroup in colon cancer, glioma and breast cancer (29–31), it is useful to accurately identify CIMP tumors without performing microarray analysis, which may reveal the etiology and clinical correlates of CIMP in AdCas. First, we examined whether the DNA methylation status of the classical CIMP markers (*p16*, *MINT1*, *MINT2*, *MINT31* and *MLH1*), which are effective for diagnosis of CIMP in colon cancer (32), reflected the methylation profile, especially CIMP, determined by MCAM analysis in AdCas (Figure 2A, left panel). CIMP-positive AdCas defined by the classical CIMP markers were not consistent with all the extensively methylated AdCas in cluster 1, suggesting that these markers are not always accurate for diagnosis of the extensively methylated AdCas.

To establish a new panel of a minimum number of CIMP markers without reducing the classification power, which was readily applied to a large number of tumor samples, we eliminated the genes from the target genes of methylation in MCAM analysis (Figure 2B). The initial definition of CIMP was based on concordant methylation of Type C loci (cancer-specific methylation) (7). Therefore, we first excluded markers that showed evidence of DNA methylation in normal tissues, which means Type A loci (age-related methylation) (7). Then, we selected 232 genes that were methylated in >75% of AdCas in cluster 1 but were methylated in <30% in the other clusters. Among these genes, 10 genes fulfilled the criteria of (i) concomitant array signals in all the probes for the same genes on the microarray, (ii) methylation-positive probes were located within 500 bp from transcription start sites and (iii) enable to design the stable and reproducible pyrosequencing assay using the candidate genes. Finally, we selected six candidate markers, *CCNA1*, *ACAN*, *GFRA1*, *EDARADD*, *MGC45800* and *p16* (*CDKN2A*), to determine CIMP in AdCas using a statistical model based on recursive descent partition analysis with the pyrosequencing data of 10 genes (33).

DNA methylation status of this panel of six markers was examined in 41 AdCas using pyrosequencing analysis. These six markers were frequently methylated in four (10%) AdCas of cluster 1, which showed DNA methylation in five or more of the six markers (Figure 2A, right panel). We designated this subgroup as CIMP-high (CIMP-H). In contrast, 26 (63%) AdCas were rarely methylated; none or one marker was methylated in this subgroup. The majority of AdCas (21 cases, 81%) in this subgroup fell into cluster 3, which showed the lowest frequency of DNA methylation. We defined AdCas with methylation in none or only one of the six markers as CIMP-negative (CIMP-N). The intermediate subgroup (11 cases, 27%) between CIMP-H and CIMP-N showed DNA methylation in two to four markers of the six selected CIMP markers. We designated this subgroup as CIMP-low (CIMP-L), in which 7 (64%) of 11 AdCas fell into cluster 2 and showed intermediate frequency of DNA methylation.

Validation analysis of newly identified CIMP markers

It is important to note that this initial selection of the six candidate markers did not introduce a bias for detecting CIMP only in the training set. Therefore, the newly identified panel of six markers was independently confirmed in a validation set of 87 AdCas. Among them, we found 6 (7%) CIMP-H, 30 (34%) CIMP-L and 51 (59%) CIMP-N tumors, which were of a similar frequency as observed in the training set of 41 AdCas (Supplementary Figure 2, available at *Carcinogenesis* Online). To estimate whether the classification by the six CIMP markers in the validation set was compatible with the CIMP classification in the training set, we performed the nearest four neighborhood prediction analysis (Figure 2C, see Materials and Methods). This

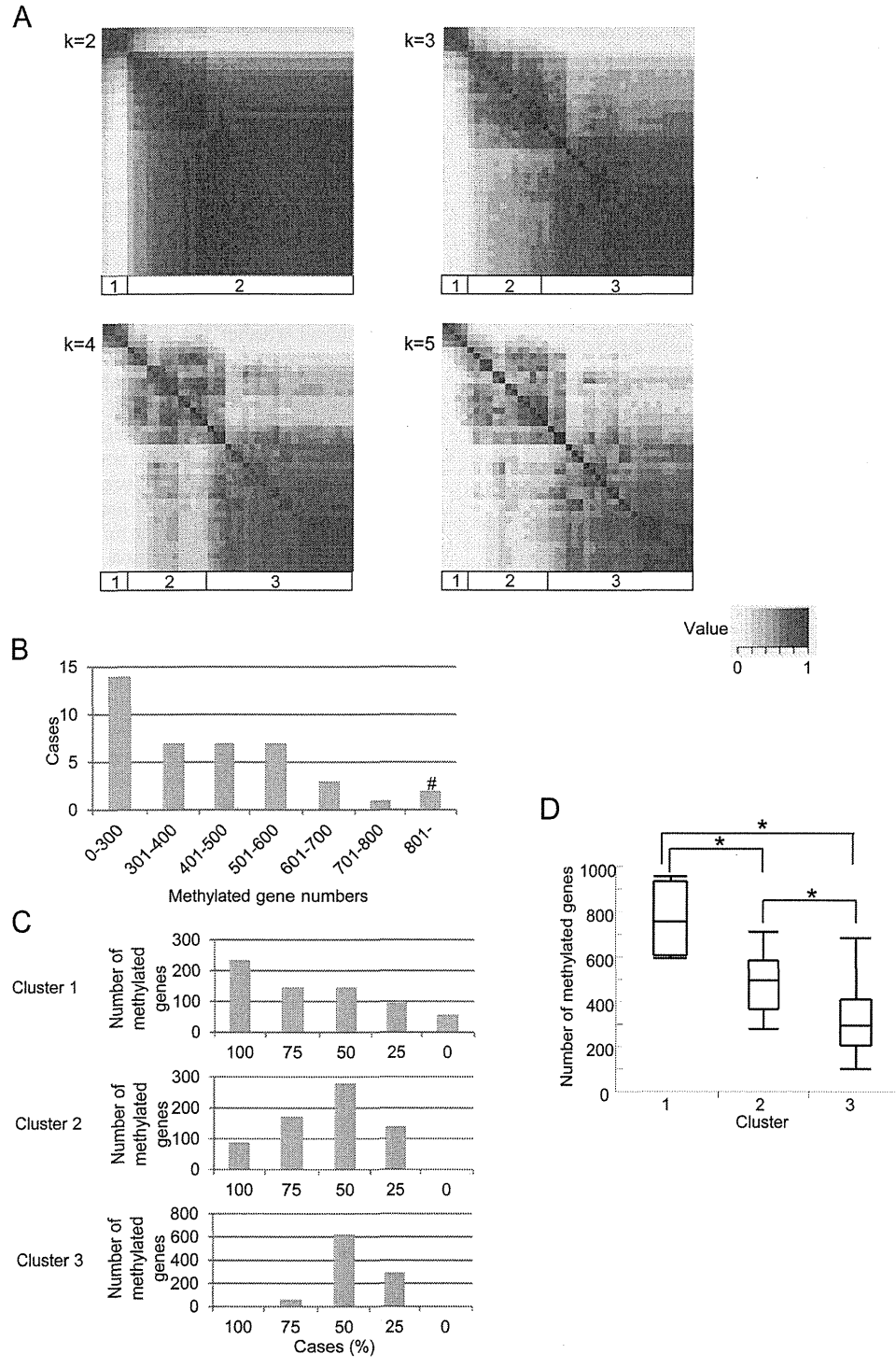

Fig. 1. DNA methylation profiling by MCAM analysis. (**A**) Consensus clustering analysis was performed with the 1156 genes from the AdCa cases for $k = 2, 3, 4$ and 5. The samples are listed in the same order on the x- and y-axes. Clusters are designated as are indicated at the bottom of each panel. Consensus index values range from 0 (highly dissimilar) to 1 (highly similar). (**B**) The distribution of number of methylated genes. X-axis indicates the number of methylated genes. Y-axis indicates cases. Two AdCas were highly methylated (#). (**C**) Distribution of number of methylated genes in each cluster. In total of 679 genes, in which methylation was observed in 20–80% of 41 AdCas, were analyzed. (**D**) Box and whisker plots of the number of methylated genes in each cluster. The mean is marked by a horizontal line inside the box whose ends denote the upper and lower quartiles. Error bars represent 5th and 95th percentile values, $^*P < 0.001$.

analysis defined 6 of 87 AdCas in the validation set as cluster 1, all of which were also categorized as CIMP-H tumors according to our criteria using the six-marker panel. Furthermore, 51 AdCas that were classified as cluster 3 with a probability >80% by the nearest neighbor classification analysis were also classified as CIMP-N tumors by our six CIMP marker panel. These results indicate that the three clusters are highly reproducible, and our panel of six markers is capable of accurately categorizing cases into these three clusters.

Identification of AdCa–CIMP in the Cancer Genome Atlas data set

Next, we examined whether the six CIMP markers could also be applicable in classifying AdCas deposited in TCGA (http://tcga-

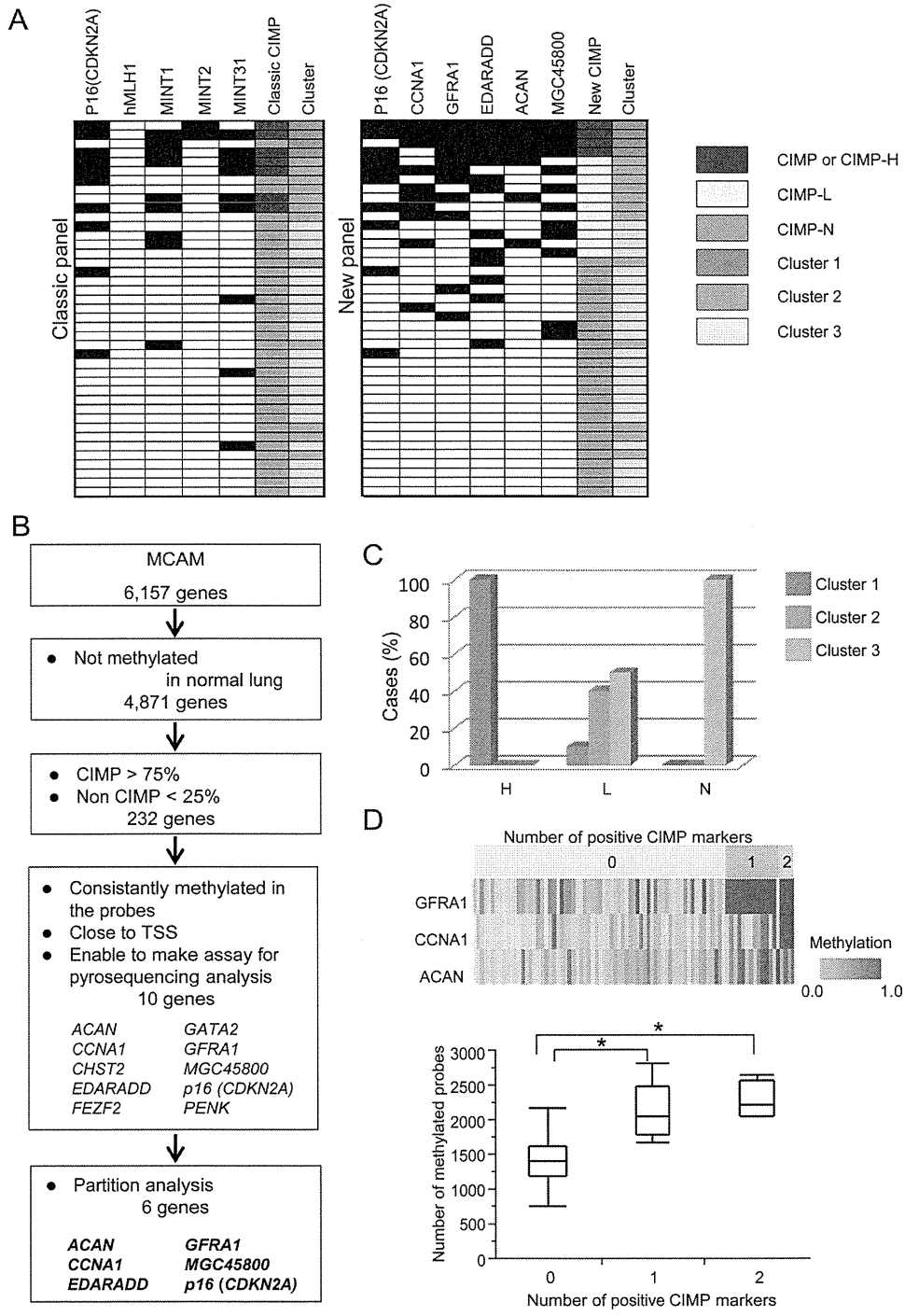

Fig. 2. DNA methylation profiling in AdCa using pyrosequencing analysis. (**A**) Comparison of classification by CIMP markers with the clusters determined by consensus clustering analysis (Figure 1A). Left: tumors with methylation in at least two of the five classical CIMP markers were determined as CIMP. Right: a panel of new CIMP markers classified CIMP-H (five or six of six markers), CIMP-L (two to four of six markers) and CIMP-N (zero or one of six markers), respectively. Black, methylation positive and white boxes, methylation negative. Clusters 1, 2 and 3 correspond to clusters 1, 2 and 3 in Figure 1A. The samples are listed in the same order on the *y*-axis in both panel. (**B**) Schema of selection for a new panel of six CIMP markers. TSS, transcription start site. (**C**) Nearest neighbor classification analysis in the validation set. Relationship between CIMP status determined by six CIMP markers, and the cluster determined by consensus cluster analysis are shown. H, CIMP-H; L, CIMP-L and N, CIMP-N. Clusters 1, 2 and 3 correspond to clusters 1, 2 and 3 in Figure 1A. (**D**) Analysis of DNA methylation status of three CIMP markers, GFRA1, CCNA1 and ACAN using the data set (3833 probes) from the Cancer Genome Atlas data set. Upper panel, heat map overview of three genes in 85 AdCas. Color corresponds to the methylation level as indicated; red is high (β value = 1.0) and yellow is low (β value = 0.0) levels of DNA methylation. Lower panel: relationship between number of methylated probes (β value > 0.4) among 3833 probes and the number of methylated genes of CIMP markers. $^{*}P < 0.001$.

data.nci.nih.gov/tcga/tcgaHome2.jsp) (30). DNA methylation data of 85 AdCas were obtained from the TCGA database, which were analyzed by the Infinium BeadChip containing 27 578 probes corresponding to 14 473 genes. Among those probes, we found that some probes corresponding to three of our new CIMP markers (*ACAN*, *CCNA1* and *GFRA1*) were located close to the regions where we conducted the pyrosequencing analysis. In contrast, no probes corresponding to the other three CIMP markers (*CDKN2A*,

MGC45800 and *EDARADD*) were located within 500 bp of transcription start sites, which was a condition of our pyrosequencing analysis. Therefore, we examined the classification power of the three CIMP markers (*ACAN*, *CCNA1* and *GFRA1*) in the 85 AdCas obtained from the TCGA. None, 4 (4.7%), 14 (16.5%) and 67 (78.8%) AdCas showed DNA methylation in three, two, one or none of the three CIMP markers, respectively (DNA methylation positive, β value > 0.4, Figure 2D, upper panel). AdCas with DNA methylation in one or two CIMP markers had more methylated probes among the 3833 most variant probes than those who had no methylation in the CIMP markers (average methylated probes: 1430.8 ± 39.5, 2116.4 ± 86.3 and 2288.8 ± 161.5, in AdCas with none, one or two methylated CIMP markers, respectively, $P < 0.001$; Figure 2D, lower panel). These data suggested that the methylation status of the three CIMP markers is also predictive for highly methylated AdCas in the TCGA data set.

Clinical significance of CIMP tumors in lung AdCa

Next, we assessed whether CIMP-positive AdCas form a distinct subgroup with characteristic clinical features. We combined two sets of AdCa cohorts (training set and validation set) for the analysis of CIMP signatures, with a total of 128 cases. We did not access any clinical information before CIMP classification of both sets of AdCas to avoid any bias in the analysis of the clinical significance of CIMP tumors. Of the 128 pooled AdCas, 10 (7.8%) were classified as CIMP-H, 40 (31.3%) as CIMP-L and 78 (60.9%) as CIMP-N (Figure 3A). CIMP-H tumors were more prevalent in males ($P = 0.0047$) and associated with frequent exposure to smoking (pack year > 40, $P = 0.0036$). Intriguingly, we found a tight association between CIMP and *EGFR* status ($P = 0.0089$; Table I). None of the 10 CIMP-H AdCas contained any *EGFR* mutations, whereas 36/78 (46.2%) CIMP-N and 12/40 (30.0%) CIMP-L AdCas had *EGFR* mutations. In contrast, no such tendency was observed between CIMP status and *KRAS*, *TP53* and *BRAF* mutations.

To investigate whether CIMP status had any impact on overall survival, we performed Kaplan–Meier survival analysis and found that CIMP-H was a significantly negative prognostic factor ($P = 0.0115$, log-rank test; Figure 3B). Since *EGFR* mutations have been indicated as a potential positive prognostic factor for survival in advanced non-small cell lung cancer patients treated with chemotherapy with or without TKI (34), we analyzed overall survival according to the *EGFR* mutation status. Among the AdCas harboring wild-type *EGFR*, CIMP-H tumors still correlated with poor survival ($P = 0.0312$, log-rank test; Figure 3C). In addition to a worse prognosis in patients with AdCas who were smokers ($P = 0.0373$, log-rank test; Figure 3D), we found that CIMP-H was an independent prognostic factor among male smokers (hazard ratio 1.7617, 95% confidence interval 1.0030–2.9550, $P = 0.0489$; Figure 3E). Taken together, these findings indicated that CIMP-H tumors have unique clinical features that distinguish them from the other AdCas.

Clinical implication of epigenetic therapy for lung AdCa

To evaluate the relationship between CIMP status and effects of the DNA methylation inhibitor, 5-Aza-dC, as an antitumor agent, we first analyzed DNA methylation status of the six CIMP markers in 14 AdCa cell lines, including one CIMP-H (H358), seven CIMP-L (H23, H1, PC9, H2009, H3255, H1975 and H1650) and six CIMP-N cell lines (H920, A549, HCC827, ML13, H1573 and HCC4011) (Supplementary Table 4, available at *Carcinogenesis* Online). CIMP-H cells (H358) harbor wild-type *EGFR*, whereas the CIMP-L and CIMP-N cells harbor either wild-type (H23, H1, H2009, H1975, H920, A549, HCC827, ML13 and H1573) or mutated (PC9, H3255, H1650 and HCC4011) *EGFR*. Regardless of the CIMP status, cells with wild-type *EGFR* showed resistance to the TKI, AG1478 (Figure 4A). Intriguingly, antitumor activity of 5-Aza-dC appeared to be associated with CIMP status. Each cell line showed different IC50, which were significantly lower in the CIMP-positive cells (average, CIMP-H and CIMP-L) than in the CIMP-N cells ($P = 0.02$, average IC50 was 68, 229 and 982 nM, respectively, Figure 4B). To determine a more accurate relationship between DNA demethylation and antitumor activity, we used level of *LINE-1* demethylation, which represents the global level of methylation, as a surrogate marker of 5-Aza-dC treatment. We examined the power of growth inhibition at a concentration of ~20% of *LINE-1* demethylation. Cell growth of CIMP-H and CIMP-L cells was significantly inhibited at each concentration of 5-Aza-dC, in contrast to CIMP-N cells, the majority of which did not respond to the treatment (Figure 4B). These data suggest that in addition to CIMP-H AdCas, tumorigenesis of CIMP-L AdCas may also depend on DNA methylation silencing pathway to some extent.

Discussion

In the current study, we performed a comprehensive genome-wide DNA methylation analysis and identified a distinct molecular subgroup (CIMP-H) in human AdCas. This subgroup showed a remarkably high rate of DNA methylation in correlated cancer-specific CpG island hypermethylation of a subset of genes, indicating the existence of CIMP in AdCas (7).

Previously, studies suggested the existence of CIMP in lung cancer. The first study defined a CIMP-positive case as having a tumor with aberrant methylation in either *CDH13* or *CRBP1* and found that CIMP-positive cases showed poorer prognosis than the CIMP-N ones (9). Although a consistent clinical feature, poor prognosis of CIMP-positive cases, was observed between our study and the previous ones, frequencies of CIMP and the other clinicopathological features associated with CIMP were varied, probably due to the different panels of CIMP marker examined (9,11–13). Thus, it is still unclear which DNA methylation markers can define the most extensively methylated subgroups (CIMP) due to the lack of accompanied genome-wide analysis in the previous AdCa studies. If CIMP affects only a subset of CpG islands in a subgroup of AdCas, collection of data for a large numbers of markers from numerous tumor samples is required to identify CIMP in AdCas. Indeed, we found in the current study that CIMP-positive tumors diagnosed by the original CIMP markers defined in the colon cancer study (7) were not consistent with the extensively methylated AdCas, suggesting that these markers are not always applicable for diagnosis of CIMP tumors other than colon cancers. Thus, the existence of CIMP in AdCas from the global point of view has remained elusive before the current study. Our genome-wide MCAM analysis successfully identified six practical and representative markers for the prediction of CIMP in AdCas.

Integrated analysis of the DNA methylation status of the six CIMP markers with several cancer-associated gene mutations, including *EGFR*, *TP53*, *KRAS* and *BRAF*, revealed that CIMP-H tumors in both the training and the validation sets did not harbor any *EGFR* mutations, suggesting that the two events are mutually exclusive, whereas mutations in the other three genes did not show such strong associations with CIMP status. Thus, our six novel markers enabled us to decipher the negative association between CIMP and *EGFR* mutations, which had been only suggested by previous studies (35). Indeed, CIMP-H tumors are significantly associated with males, frequent exposure to smoking and high relapse rate of disease, which clearly differ from the typical features of *EGFR*-mutant AdCas, such as association with females, non-habit forming smoking and better prognosis. Interestingly, colorectal cancers also show strong association between CIMP status and smoking (36,37). Thus, smoking may be one of the potential causes of CIMP. These data suggested that a particular set of genes are methylated in CIMP-H AdCas, and their target genes are involved in activation of an alternative pathway, in which tumorigenesis may be minimally dependent on *EGFR* mutation.

The association of better clinical outcome with CIMP-positive tumors has been reported in breast cancer, colon cancer and glioma. Fang *et al.* (31) showed that there was significant overlap of CIMP targets in those different types of cancers. Among the 33 overlapped CIMP targets between the cancers, we found that the DNA methylation status of 19 genes was available from our MCAM analysis. Using

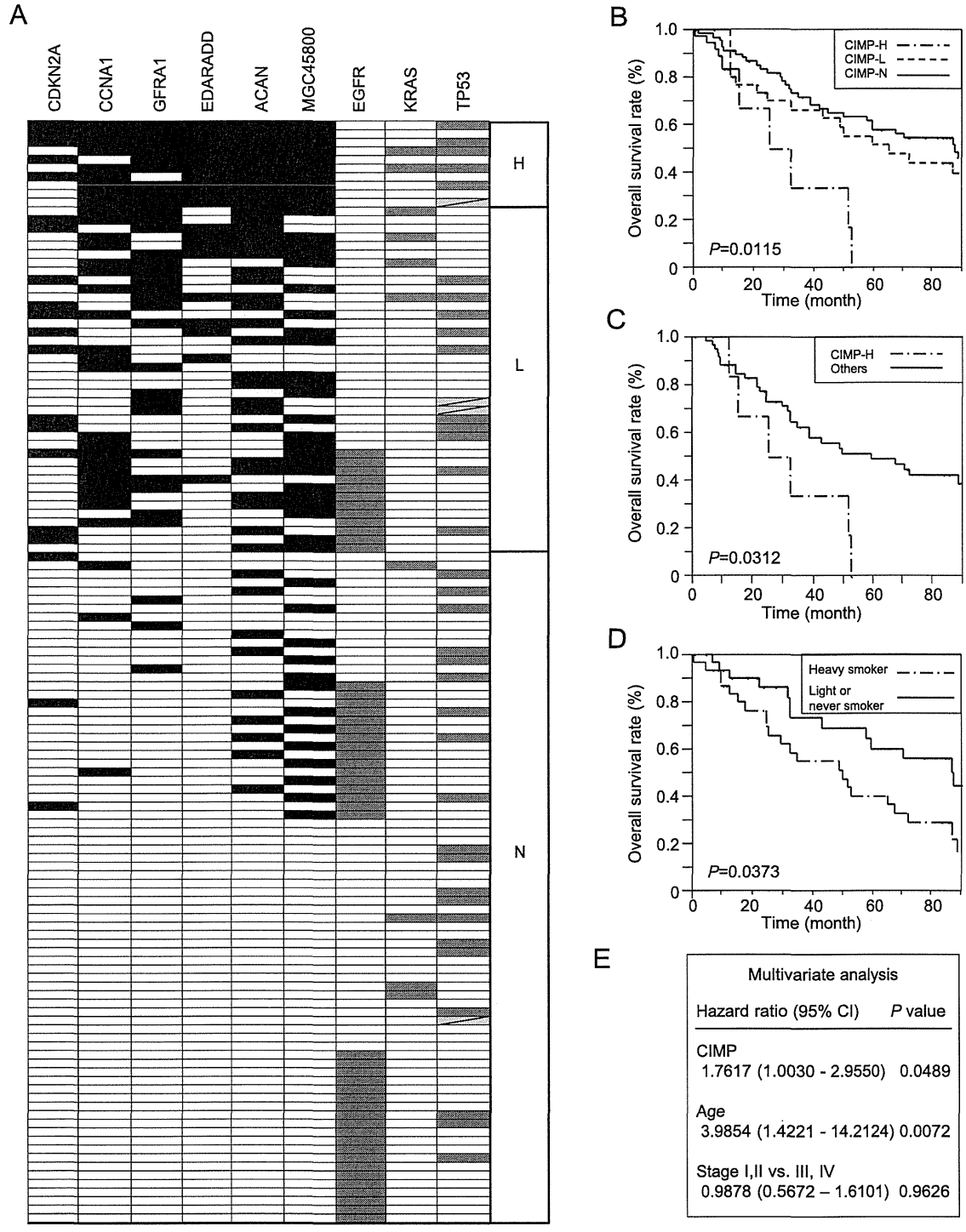

Fig. 3. CIMP status associated with prognosis of AdCas. (**A**) Total of 128 AdCas were classified into three subclasses by the six newly identified CIMP markers. Black boxes, methylation positive; gray boxes, mutation positive; white boxes, methylation negative or mutation negative and light gray boxes with oblique lines, data were not available for *TP53* status. H, CIMP-H; L, CIMP-L and N, CIMP-N. (**B**) Kaplan–Meier analysis for overall survival of 128 AdCa patients by CIMP status. *P* value was calculated by log-rank analysis. (**C**) Kaplan–Meier analysis for overall survival of 80 AdCas cases harboring wild-type *EGFR* by CIMP status. (**D**) Kaplan–Meier analysis for overall survival by smoking status. (**E**) Multivariate analysis showed that CIMP-H was an independent prognostic factor among male smokers ($n = 37$).

the methylation status of these 19 genes, we found that AdCas in our training set were divided into three clusters; the three most extensively methylated AdCas were consistent with the CIMP-H AdCas, suggesting that a panel of 19 genes may also be a potent predictor for CIMP-H in AdCas (Supplementary Figure 3, available at *Carcinogenesis* Online). However, given the worse prognosis of patients with CIMP-H AdCas, the impact of CIMP to survival in lung cancer might be different from the CIMP in colon cancer, glioma and breast cancer. Indeed, a study in myelodysplastic syndromes also showed that the presence of CIMP was significantly associated with poor prognosis and risk of leukemia transformation (38). The contrasting impacts of CIMP to clinical outcome might be due to the distinct DNA methylation profiles specific to each tumor type; CIMP confers poor prognosis in lung AdCas and myelodysplastic syndromes via inactivation